investigation included Thy-1, owing to its characteristics as a cell surface marker expressed on vascular endothelial cells (EC) that are upregulated by the inflammatory cytokines interleukin (IL)–1β and tumor necrosis factor (TNF)–α.[18] Endostatin is an endogenous angiogenesis inhibitor that is activated by proteases such as those derived from inflammatory cells.[19-21] The antigen Ki-67 was used as a nuclear marker of cell proliferation.[22]

METHODS

PATIENTS AND TREATMENTS

We retrospectively reviewed 38 eyes of 38 consecutive AMD patients in different centers who were surgically treated with full macular translocation surgery with CNVM extraction. All patients had clinically active disease and progression. Fourteen CNV patients without any kind of therapy prior to surgery composed the control CNV group. The clinical characteristics of these 14 patients are summarized in **Table 1**. Twenty-four patients received surgery following intravitreal bevacizumab injection (bevacizumab CNV group). Therapy options, including observation, conventional thermal laser photocoagulation, verteporfin PDT, intravitreal injection of triamcinolone acetonide or anti-VEGF agents, and full macular translocation with 360° retinotomy and CNVM extraction were discussed with the patients. Although submacular removal of CNV was not favored by the randomized submacular surgery trials, submacular surgery trial Group B revealed that submacular surgery for predominantly hemorrhagic CNV did reduce the risk of severe visual acuity loss (loss of ≥6 Early Treatment Retinopathy Study lines) and contrast sensitivity loss (≥3 segments, using the Pelli-Robson chart at 0.5 m) significantly, in comparison to the group observed without any treatment for 24 months of follow-up.[23] Macular translocation of the retina, a complex but potentially effective surgical method, was reported to be beneficial when CNV was related to submacular hemorrhage[24] or RPE tear.[25] Furthermore, improvement in distance and near visual acuity as well as in reading speed was detected at the 1-year follow-up of patients with neovascular AMD who were treated with macular translocation.[26,27]

Intravitreal bevacizumab injection and surgical intervention with full macular translocation surgery were offered when (1) visual acuity was worse than 20/200 (being the minimum visual acuity to recommend the first PDT, according to the Treatment of Age-Related Macular Degeneration with Photodynamic Therapy investigation[28,29]); (2) CNV was related to retina pigment epithelium (RPE) tear, chorioretinal anastomosis, or massive subretinal/intravitreal hemorrhage; (3) visual deterioration progressed and subretinal hemorrhage and RPE tear appeared following treatment; or (4) reading ability was recently lost, despite improvement in distant visual acuity after previous treatment. The clinical characteristics of the patients treated with intravitreal bevacizumab are summarized in **Table 2**. Reduction of intraoperative bleeding was intended with the preoperative injection of bevacizumab, as suggested in other ocular pathologies.[30-33]

Each patient gave written informed consent regarding their knowledge of the off-label use and experimental nature of the treatment procedure, and the risks and benefits of all therapeutic options were discussed in detail. The study followed the guidelines of the declaration of Helsinki. Local institutional review board approval was granted for allocation and histological analysis of the specimens.

TISSUE PREPARATION AND IMMUNOHISTOLOGY

Within minutes after surgery, excised CNVM were fixed in 3.7% formalin and embedded in paraffin. After serial sections were deparaffinized and rehydrated, antigen retrieval was accomplished by proteolytic digestion with 0.5% protease XXIV (Sigma, St Louis, Missouri) for cytokeratin 18, endostatin, and Thy-1, and by heat treatment in citrate buffer in a pressure cooker under 120°C for 2 minutes for Ki-67, CD45, CD68, ICAM-1, and E-selectin.

Table 1. Clinical Characteristics of Patients Without Any Kind of Preoperative Therapy

Patient, No./ Sex/Age, y	Eye	CNV Type
1/F/71	Right	Hemorrhagic
2/F/80	Right	Occult with hemorrhage
3/F/75	Left	Predominantly classic
4/M/75	Right	Classic with hemorrhage
5/F/75	Right	Classic with hemorrhage
6/F/76	Right	Hemorrhagic
7/M/80	Left	Hemorrhagic
8/M/80	Left	Hemorrhagic
9/M/72	Left	Classic with hemorrhage
10/F/73	Right	Hemorrhagic
11/F/74	Left	Occult with hemorrhage
12/F/81	Right	Hemorrhagic
13/M/80	Left	Hemorrhagic
14/M/64	Right	Occult

Abbreviation: CNV, choroidal neovascularization.

Immunohistochemical staining with the primary mouse monoclonal antibodies specific for cytokeratin 18 (Progen, Heidelberg, Germany), ICAM-1 (Novocastra, Newcastle upon Tyne, England), E-selectin (Novocastra), CD45 (Dako, Glostrup, Denmark), and Ki-67 (Clone Ki-S5; Dako) was performed using the avidin-biotin complex horseradish peroxidase method, as previously described.[34] For E-selectin, cytokeratin 18, and ICAM-1 staining, the brown chromogen 3-diaminobenzidine was replaced with 3-amino-9-ethylcarbazole, a highly sensitive substrate chromogen (Code K3461; Dako).

Immunohistochemical staining for Thy-1, CD68, and endostatin was performed by the alkaline-phosphatase method, according to the manufacturer's instructions (ChemMate Detection Kit, Alkaline Phosphatase/RED, Rabbit/Mouse, K5005; Dako), as previously described,[34] using primary antihuman antibodies specific for Thy-1 (mouse anti-CD90 antibody; BD Biosciences Pharmingen, San Jose, California), CD68 (mouse, monoclonal; Dako), and endostatin (rabbit, polyclonal; Dianova GmbH, Hamburg, Germany). Color was developed using chromogen red (ChemMate Detection Kit; Dako). Hematoxylin (Chemmate, Code S2020; Dako) was used for counterstaining.

For negative controls, primary antibodies were substituted by the appropriate normal sera or omitted.

ANALYSIS

Serial sections from a specimen were analyzed by light microscopy.

Immunoreactivity for ICAM-1, E-selectin, CD68, and endostatin was analyzed semiquantitatively and separately in the RPE, EC (in the perivascular area for CD68), and stroma. A grading scheme indicating the degree of labeling was used: numerals 3, 2, 1, and 0 were assigned for intense (70%-100% positive cells), moderate (40%-69% positive cells), weak (1%-39% positive cells), and absent of staining, respectively.

Each specimen was documented under ×50 magnification with a Zeiss microscope (Axioskop; Carl Zeiss, Inc, Oberkochen, Germany) connected to a digital camera (Fujix HC-300Z; Fujifilm, Tokyo, Japan). The area of each specimen was measured using the appropriate hardware and software (AxioVision, Version 3.1, Carl Zeiss, Inc, Göttingen, Germany).

Table 2. Clinical Characteristics of Patients Treated With Intravitreal Bevacizumab Before Submacular Surgery

Patient, No./ Sex/Age, y	Eye	CNV Type	No. of Bevacizumab Injections	Time to Surgery From Treatment, d	
				PDT	Intravitreal Bevacizumab
1/F/80	Left	Hemorrhagic	1	-	1
2/F/86	Left	Hemorrhagic	1	-	3
3/M/75	Right	Occult hemorrhagic with RPE tear	1	-	3
4/M/69	Left	Occult	1	-	4
5/M/69	Left	Occult	1	-	4
6/F/71	Right	Hemorrhagic	1	-	6
7/M/83	Right	Hemorrhagic PED	1	-	6
8/M/79	Left	Predominantly classic with CRA	1	-	7
9/M/74	Right	Hemorrhagic	1	-	9
10/F/69	Right	Hemorrhagic with RPE tear	1	-	11
11/F/73	Left	RPE tear	1	-	12
12/F/72	Right	Hemorrhagic occult	1	39	12
13/M/73	Left	RPE tear	1	-	26
14/M/58	Right	Hemorrhagic with RPE tear	1	-	43
15/F/79[a]	Right	Hemorrhagic with RPE tear	1	343	43
16/F/85	Right	Occult with PED	1	-	44
17/F/81	Right	Hemorrhagic with RPE tear	1	-	46
18/M/79	Left	Predominantly classic	1	64	48
19/M/78	Left	Occult hemorrhagic	5	249	209/167/125/92/50
20/F/76	Left	Hemorrhagic	1	-	53
21/M/79	Right	Occult with RPE tear	2	-	95/55
22/M/75	Right	Occult	1	-	57
23/F/84	Right	Hemorrhagic with PED	2	-	135/85
24/F/75	Right	Predominantly classic	2	-	154

Abbreviations: CNV, choroidal neovascularization; CRA, chorioretinal anastomosis; PED, pigment epithelial detachment; PDT, photodynamic therapy; RPE, retina pigment epithelium.

[a]Patient was treated with an intravitreal triamcinolone acetonide injection 342 days before surgery.

All Ki-67–positive nuclei, macrophages, and leukocytes were counted in each specimen. Proliferative activity, density of leukocytes, and macrophage infiltration in each specimen were determined quantitatively by calculating the ratio of the total number of Ki-67 positive nuclei, macrophages, and leukocytes in the CNVM to the total area of the membrane.

Thy-1 expression was determined by the percentage of Thy 1–expressing vessels in the overall vascularization of each membrane.

Intensity of CD68, ICAM-1, E-selectin, and endostatin immunostaining, density of leukocyte and macrophage infiltration, proliferative activity, and Thy-1 expression in the described CNV groups were compared using the Mann-Whitney *U* test. Immunohistologic findings in the bevacizumab CNV group were analyzed based on timing or number of bevacizumab injections, using the Spearmann correlation test. A *P* value less than .05 was considered significant.

RESULTS

Immunohistological findings are summarized in **Figure 1**

HISTOPATHOLOGICAL FINDINGS IN THE CONTROL CNV GROUP

Retina pigment epithelial cells immunoreactive for cytokeratin 18 were found in all specimens.

All but 1 membrane was vascularized. Immunohistological stains of the specimen from a patient with massive subretinal hemorrhage (**Figure 2**A) are shown in Figure 2.

Expression of E-selectin was found in the RPE of all CNVM, and intensely in 4 (28.6%) membranes. E-selectin was detected in the EC of 8 CNVM (57.1%) and in the stroma of 9 CNVM (64.3%) (Figures 1A and 2B).

Expression of ICAM-1 was prominent in the RPE; it was intense in 13 CNVM (92.9%). No ICAM-1 was present in the EC of 9 CNVM (64.3%). Intense ICAM-1 expression was detected in the EC of 3 (21.4%) and in the stromal cells of 2 CNVM (14.3%) (Figures 1B and 2C).

Leukocytes detected by CD45 immunostaining were found to be present in all but 1 CNVM. The number of leukocytes in a 1-mm^2 area of CNVM varied between 0 and 779.6 (median, 106.64 cells/mm^2) (Figure 1C). The specimen in Figure 2D has the fourth highest density of leukocyte infiltration (157.39 cells/mm^2) in the control CNV group.

The density of macrophages ranged between 183.94 cells/mm^2 and 2826.73 cells/mm^2 (median, 882.66 cells/mm^2) (Figure 1C). Macrophage infiltration was seen in the RPE cell layer, the perivascular area, and the stroma in 85.7% (n=14), 61.5% (n=13), and 92.8% (n=14) of the specimens. Intense macrophage infiltration was detected in the RPE cell layer of 6 (42.8%), the perivascular area of 2 (14.3%), and the stroma of 4 (28.6%) CNVM (Figures 1D and 2E).

Vessels expressing Thy-1 were detected in 13 of 14 specimens (92.8%), in varying percentages of vessels (median, 80.0%; range, 0%-100%). In 4 (28.6%) CNVM, all vessels displayed Thy-1 (Figure 2F).

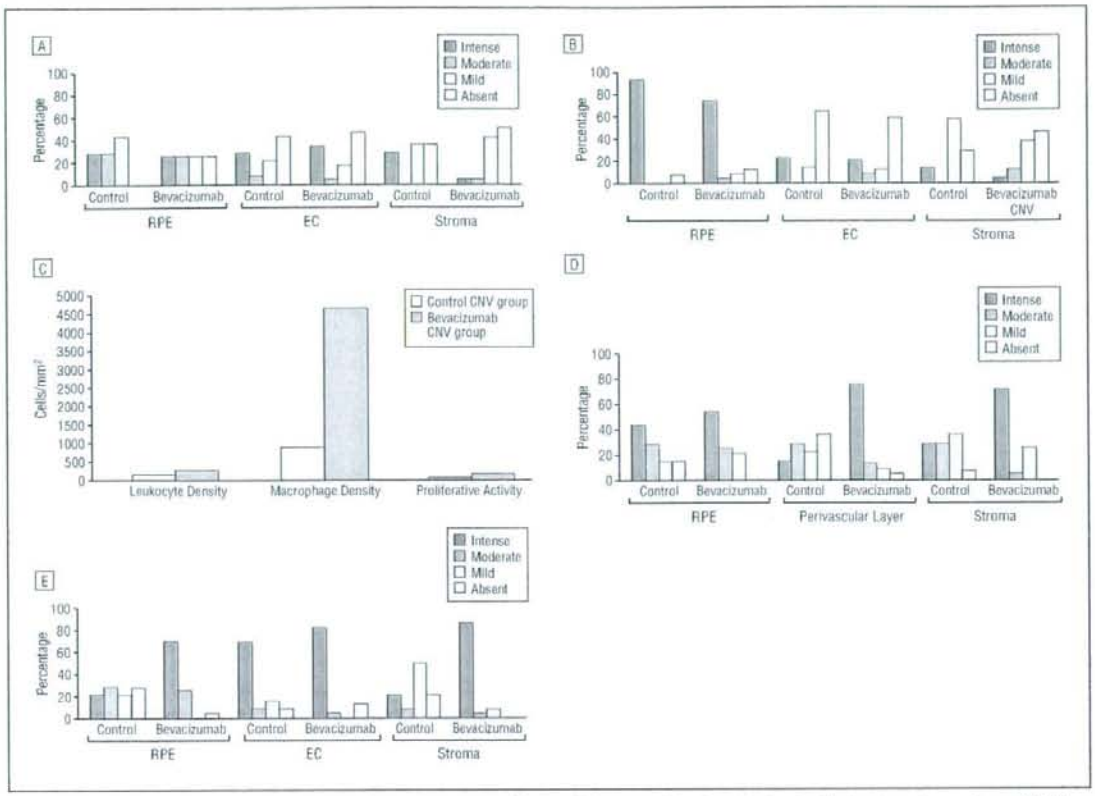

Figure 1. Graphs showing E-selectin (A) and intercellular adhesion molecule (ICAM)–1 (B) immunostaining intensity, density of leukocytes and macrophages (CD68) and proliferative activity (C), CD68 immunoreactivity (D), and intensity of endostatin staining (E) in choroidal neovascular membranes (CNVM) without any kind of previous therapy (control choroidal neovascularization [CNV] group) and CNVM excised after intravitreal injection of bevacizumab (Avastin; Genentech, Inc, South San Francisco, California) (bevacizumab CNV group). Expression of ICAM-1, E-selectin, CD68, and endostatin immunostaining in retina pigment epithelium (RPE), endothelial cells (EC) (perivascular area for CD68), and stroma were evaluated separately and semiquantitatively as intense (70%-100% positive cells), moderate (40%-69% positive cells), mild (1%-39% positive cells), or absent (A,B,D,E). All Ki-67–positive nuclei, CD45-immunoreactive leukocytes, and CD68-immunopositive macrophages were counted in each specimen. Proliferative activity and density of leukocytes and macrophages were determined separately for each CNVM by the ratio of total number of proliferating cells, leukocytes, and macrophages to the total area of the membrane (mm^2); their median values were shown in (C).

Immunoreactivity to endostatin was detected in the RPE–Bruch membrane complex in 10 (71.4%) membranes. Endostatin was immunonegative in vessels in only 7.7% (n=1) of the specimens. Within the stroma, endostatin was expressed by fibroblast-like and inflammatory cells in 11 (78.6%) specimens (Figures 1E and 2G).

Proliferative activity varied between 6.67 and 514.08 Ki-67–expressing nuclei/mm^2 (median, 34.34 nuclei/mm^2) (Figure 1C). Proliferating cells belonged mostly to inflammatory infiltrate within the stroma (Figure 2H). In 12 (85.7%) CNVM, proliferative activity was less than 160 Ki-67–expressing nuclei/mm^2. The specimen in Figure 2H has the second highest proliferative activity among the control CNV group (511.05 nuclei/mm^2).

HISTOPATHOLOGICAL FINDINGS IN THE BEVACIZUMAB CNV GROUP

In the bevacizumab CNV group (**Figure 3**A), the RPE had E-selectin in 18 (75.0%) CNVM. The EC were E-selectin immunonegative in 11 (45.8%) CNVM. Intense E-selectin staining was detected in the RPE of 6 (25%) and the EC of 8 (33.3%) CNVM. Stromal cells expressed E-selectin in 12 (50.0%) CNVM (Figures 1A and 3B). Expression of E-selectin in the bevacizumab CNV group was comparable to the control CNV group.

Immunoreactivity for ICAM-1 was detected in the RPE of 21 CNVM (87.5%) and intensely in 18 CNVM (75%). Intense ICAM-1 expression was found in the EC of 5 (20.8%) and stromal cells of 1 (4.2%) CNVM (Figures 1B and 3C). Expression of ICAM-1was not significantly different from the control CNV group.

Leukocytes were found in all specimens (median, 271.61 cells/mm^2; range, 33.50-2351.01 cells/mm^2) (Figure 3D). The density of leukocytes seemed higher than in the control group, but without statistical significance (Figure 1C, $P=.07$).

Macrophages were present in all CNVM (median, 4661.95 cells/mm^2; range, 321.01-61821.16 cells/mm^2) (Figures 1C and 3E). The density of macrophages was significantly higher than that of the control CNV group ($P<.001$). Moderate to strong macrophage infiltration was detected within the RPE cell layer and in the perivascular area in 18 (75%) specimens and in the stroma in 17 (70.8%)

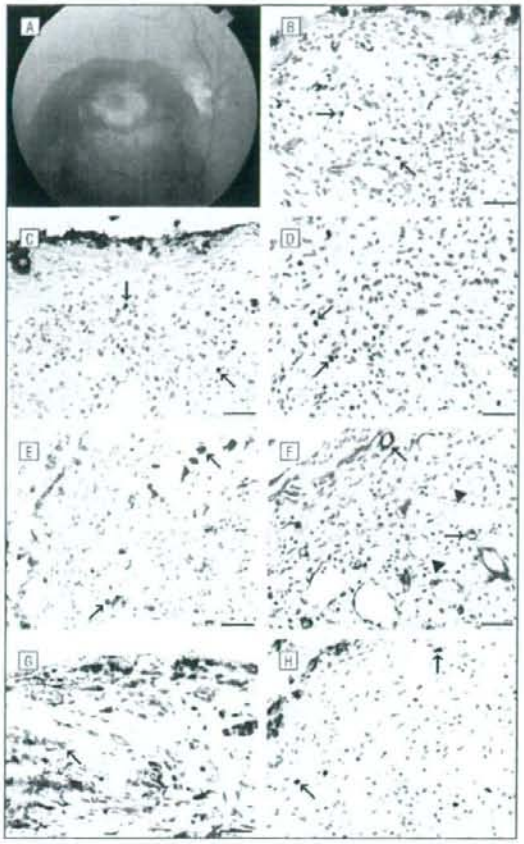

Figure 2. Color fundus (A) and histologic photomicrographs (B-H) of a choroidal neovascularization membrane (CNVM) extracted without any kind of therapy before surgery. Note the massive subretinal hemorrhage (A). Sections were probed with antibodies against E-selectin (B), intercellular adhesion molecule (ICAM)–1 (C), CD45 (common leukocyte antigen; D), CD68 (E; macrophages), Thy-1 (F), endostatin (G), and Ki-67 (H). Sections were stained with 3-amino-9-ethylcarbazole red chromogen (B, C), 3-diaminobenzidine resulting in a brown chromogen (D, H), and red chromogen (E-G). Hematoxylin was used as a counterstain. B, E-selectin expression is prominent in endothelial cells (EC, arrows). ICAM-1 expression (C) was detected in the retina pigment epithelium (RPE, asterisk) and stromal cells (arrows). Leukocytes (D, arrows) and macrophages (E, arrows) were present in perivascular area and stroma. Besides Thy-1–expressing vessels (F, arrows), some Thy-1–immunonegative vessels (arrowheads) were found in the same specimen. Endostatin (G) was found to be weakly present in some vessels (arrow) whereas the RPE (asterisks) was endostatin immunonegative. H, Some proliferating cells (arrows) were present in the CNVM. Scale bars = 50 μm.

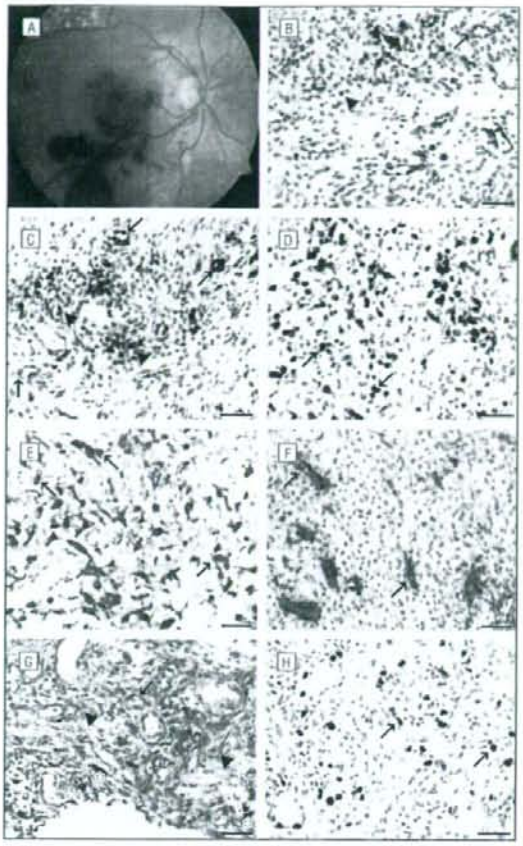

Figure 3. Histologic photomicrographs of the choroidal neovascularization membranes extracted 4 days after intravitreal bevacizumab injection. Note the massive subretinal hemorrhage with pigment epithelium detachment (A). Sections were probed with antibodies against E-selectin (B), intercellular adhesion molecule (ICAM)–1 (C), CD45 (common leukocyte antigen; D), CD68 (macrophages; E), Thy-1 (F), endostatin (G), and Ki-67 (proliferating cells; H). Sections were stained with 3-amino-9-ethylcarbazole red chromogen (B, C), 3-diaminobenzidine resulting in a brown chromogen (D, H), or red chromogen (E-G). Hematoxylin was used as counterstain. Endothelial cells (arrows) and stromal cells (arrowheads) showed E-selectin (B) and ICAM-1 (C). Inflammatory infiltration with many leukocytes (D, arrows) and many macrophages (E, arrows) was detected within the perivascular area and stroma. Expression of Thy-1 was intensely expressed in vascular structures (F, arrows). G, Endostatin was intensely immunopositive in vessels (arrow), stromal cells (arrowheads), and retina pigment epithelium (asterisks). Many cells within the stroma expressed Ki-67 (H, arrows). Scale bars = 50 μm.

CNVM (Figure 1D). Immunoreactivity of CD68 was significantly more intense in the bevacizumab CNV group in the perivascular area (median, 3) and stroma (median, 3) than in the control CNV group (median, 1; $P < .001$ and median, 2; $P = .03$, respectively).

In the CNVM of all patients treated with bevacizumab, all vessels were lined with EC displaying Thy-1 (median, 100.0%) (Figure 3F). The percentage of Thy-1–expressing vessels was significantly higher in the bevacizumab CNV group ($P < .001$).

The RPE–Bruch membrane complex displayed endostatin in all but 1 CNVM either strongly (70.8%; n = 17) or moderately (25.0%; n = 6). Endostatin was intensely expressed in the vessels of 20 CNVM (87.3%). Stromal cells displayed endostatin in all CNVM and strongly in 21 (87.5%) membranes (Figures 1E and 3G). Endostatin was significantly stronger in the RPE–Bruch membrane complex (median, 3; range, 2-3; $P < .001$) and stroma (median, 3; range, 1-3; $P < .001$) of the bevacizumab CNV group than the control CNV group (median, 1 5; range, 0-3 and median, 1; range, 0-3, respectively).

Proliferative activity (median, 204.33 cells/mm^2; range, 3.61-1886.135 cells/mm^2) in the bevacizumab CNV group was significantly higher than that in the control CNV group ($P = .007$) (Figures 1C and 3H).

Table 3. Evaluation of Histopathological Findings in Bevacizumab CNV Group With Regard to Application of Becavizumab and PDT[a]

	Based on Timing of Injections		Based on Frequency of Injections		Based on Previous Treatment				
					With PDT		Without PDT		
	P Value	ρ	*P* Value	ρ	Median	Range	Median	Range	*P* Value
E-selectin									
RPE	.07	0.38	.62	−0.10	1	1-3	2	0-3	>.99
EC	.39	0.18	.73	0.07	2	1-3	0	0-3	.04
Stroma	.86	−0.04	.93	−0.02	0.5	0-1	0.5	0-3	.86
ICAM-1									
RPE	.81	0.05	.88	0.03	3	0-3	3	0-3	.88
EC	.71	0.08	.76	0.07	0	0-2	0	0-3	.39
Stroma	.81	0.05	.57	−0.12	0.5	0-1	1	0-3	.61
Density of leukocytes	.25	−0.24	.86	−0.04	107.83	50.49-165.12	383.77	33.50-2351.10	.09
Density of macrophages	.64	−0.099	.96	0.01	4085.5	321.01-5078.1	4951.91	1308.57-61821.16	.28
Thy-1	>.99		>.99		100	100-100	100	100-100	>.99
Endostatin									
RPE	.94	0.02	.20	0.27	3	3-3	3	2-3	.28
EC	.35	0.21	.50	0.15	3	2-3	3	0-3	.27
Stroma	.39	0.18	.42	0.17	3	1-3	3	1-3	.38
Proliferative activity	.09	−0.36	.22	−0.26	128.72	3.61-198.73	160.19	25.12-1886.14	.28

Abbreviations: CNV, choroidal neovascularization; CNVM, choroidal neovascular membrane; EC, endothelial cells; ICAM, intercellular adhesion molecule; PDT, photodynamic therapy; RPE, retina pigment epithelium.

[a] Intensity of E-selectin, ICAM-1, and endostatin immunostainings in RPE, EC, and stroma. Density of leukocyte and macrophage infiltration, proliferative activity, and Thy-1 expression in bevacizumab CNVM were analyzed based on timing or number of bevacizumab injections with the Spearmann correlation test and compared based on previous application of verteporfin PDT using the Mann-Whitney *U* test. $P < .05$ was considered significant.

Immunohistologic findings in the bevacizumab CNV group did not show major differences based on either timing or number of bevacizumab injections (**Table 3**). Based on previous application of PDT, only E-selectin expression showed a major difference, being significantly stronger in the EC of patients in the bevacizumab CNV group treated with PDT previously (n=4) than those in the bevacizumab CNV group without any previous PDT (n=20) (Table 3).

COMMENT

Vascular endothelial growth factor is expressed in the choroid of human eyes,[35,36] and polarized secretion of VEGF in the RPE is vital for choriocapillaris development and maintenance.[37] In AMD, various factors such as free radicals or complement components may upregulate VEGF expression.[38,39] Vascular endothelial growth factor, chemotactic for inflammatory cells, activates monocytes and macrophages and induces expression of ICAM-1 and E-selectin on vascular EC to facilitate adhesion and migration of inflammatory cells.[15-18,20,40] Macrophages synthesize the cytokines IL-1 and TNF-α,[20,41-43] which enhance ICAM-1 expression in EC and in the RPE,[44-46] and induce inflammatory cell infiltration further. There is a closed but amplifying circuit between VEGF and inflammatory cells, because leukocytes and macrophages can produce VEGF themselves and also induce VEGF production in the RPE through IL-1 and TNF-α in human CNVM.[13,20,47-49] Vascular endothelial growth factor, in turn, stimulates growth and maintenance of the CNVM.[12,50-52] Because VEGF and inflammation seem to closely interact with each other, VEGF inhibition by bevacizumab might influence, or possibly inhibit, the inflammatory activity in CNV.

In the specimens treated with bevacizumab, expression of ICAM-1 and E-selectin was comparable to that of the control CNV cases without previous therapy. However, density of leukocytes, and especially of macrophages, was higher in the bevacizumab CNV group than in the control CNV group. Consequently, the percentage of Thy-1–expressing vessels, a mirror of TNF-α and IL-1 activity, was also significantly higher. Macrophages, reported to be present in 60% of the surgically excised CNVM,[12] seem to play a causative role in neovascular AMD pathogenesis.[48,49] In aged RPE cells, accumulation of oxidation products seems to induce angiogenic and chemotactic factors like monocyte chemoattractant protein 1.[53] In healthy human eyes, recruited macrophages may have a physiological role in removing the accumulated subretinal debris. However, excess oxidized lipids in the eyes of patients with AMD were suggested to upregulate the release by macrophages of proteolytic enzymes that damage the Bruch membrane and contribute to CNV development.[54] Macrophages, in addition to stimulating VEGF, can induce EC proliferation and migration through the release of cytokines, proteases, and growth factors.[20] Therefore, experimental studies for potential new antiangiogenic treatment strategies target the complement system,[55] ICAM,[56] macrophages, monocytes,[48,49] and TNF.[57] These were shown to inhibit leukocyte infiltration and VEGF expression and, therefore, inhibit CNV development or progression in experimental studies.[48,49] In experimental models, early intravitreal injection of VEGF-A antibody after CNV induction was shown to inhibit CNV and choroidal macrophage in-

filtration through suppression of monocyte chemoattractant protein 1 expression in the RPE-choroid complex.[58] Hence, anti-VEGF drugs might be expected to have an anti-inflammatory effect.[59]

Our results were truly unexpected. Inhibition of VEGF with bevacizumab was related to a prominent inflammatory reaction, instead of an anti-inflammatory effect, in comparison to the control CNV group. This might be for several reasons.

First, the Fc portion of bevacizumab in CNV may stimulate a cellular immune response through Fc receptors in immune cells. Bevacizumab was shown to penetrate the retina in an experimental study.[60] Anatomical defects in the Bruch membrane created by proteolytic enzymes and CNV itself might facilitate the passage of bevacizumab molecules through the RPE to the CNVM in the eyes of patients with AMD.

Second, VEGF acts as a survival factor for EC by inhibiting apoptosis.[37,61] Deprivation and/or inhibition of VEGF was shown to induce vascular regression through EC apoptosis, especially in neovascular vessels.[61-65] During vascular regression, macrophages regulate EC and pericyte apoptosis in capillaries. Leukocytes release human neutrophil peptides that are proapoptotic for EC.[66] Macrophages also recognize and phagocytose apoptotic cells. Macrophage depletion results in EC survival and persistence of functional capillaries.[67-69] Therefore, increased inflammatory cell infiltration following bevacizumab injection may reflect part of the vascular regression process in CNV, based on debris removal by macrophages.

Third, macrophages might be involved in CNV inhibition. In mice deficient in monocyte chemoattractant protein 1 or its receptor, accumulating complement factors or IgG stimulated VEGF expression in the RPE and, therefore, CNV development.[59] In another experimental study, inhibition of macrophage entry into the eye stimulated CNV, whereas direct injection of macrophages inhibited CNV.[70] Previously, macrophage depletion with liposomal clodronate was shown to inhibit CNV development.[48,49] However, reduction of neovascularization in these studies was recently suggested to be due to the direct toxicity of liposomes on EC rather than macrophage depletion itself.[70]

Last, inflammatory cells are known to contribute to antiangiogenesis through activation of endogenous angiogenesis inhibitors such as endostatin. Macrophages and leukocytes release proteases such as matrix metalloproteases.[20] Proteases cleave endostatin that is bound to collagen XVIII in vascular basement membranes and the Bruch membrane. Through this cleavage, endostatin is released and activated.[21] In our series, endostatin was significantly more intense in the RPE and stroma of the inflammatory active bevacizumab CNV group than in the control CNV group. This has important consequences because endogenous endostatin was shown to inhibit CNV.[19] Furthermore, endostatin was decreased in the RPE and choroid of human eyes with AMD, and its deficiency was suggested to predispose CNV formation.[71]

Vascular endothelial growth factor was shown to be an important mitogenic factor for choroidal EC[37,47,72,73] and also for RPE cells.[74] However, whether anti-VEGF toxins or antibodies inhibit proliferation of human choroidal and RPE cells is controversial in in vitro settings.[75-77] Recently, we have shown the antiproliferative effect of bevacizumab on EC in in vitro studies.[78,79] Still, in vitro results may not reflect the ongoing process in vivo. In the bevacizumab CNV group, proliferative activity was significantly higher than in the control CNV group. Proliferating cells were located within the stroma and originated from the inflammatory infiltrate rather than the RPE or EC. In our previous work, proliferative activity was correlated with inflammatory activity, and was significantly higher in inflammatory active specimens than in inflammatory inactive ones.[34,80]

In our series, timing of the bevacizumab injection prior to surgery varied between 1 and 154 days. Four of the 24 patients were treated with 2 to 3 bevacizumab injections preoperatively. However, immunohistologic findings in the bevacizumab CNV group did not show major differences based on timing or number of injections. Four of the patients were treated with PDT 39 to 343 days before bevacizumab injection. Of the antigens investigated, only E-selectin was found to be significantly more intense in the EC of the bevacizumab CNV patients treated previously with PDT. However, our previous studies[34] have shown that immunohistopathological findings dramatically change early (3 days) after PDT when compared with either longer intervals following PDT or the control CNV group. The implications of PDT-bevacizumab combination therapy on inflammation and angiogenesis, therefore, need to be evaluated in a higher number of samples excised early after combination therapy.

To our knowledge, this is the first clinicopathological study evaluating inflammation and proliferation in human CNV treated with an anti-VEGF agent. To interpret the results properly, the following limitations need to be taken into account: first, histopathological specimens reflect only a time window within a dynamic process. Therefore, we selected homogenous control and treatment groups that were comparable in their clinics. Second, in contrast to experimental studies, time between treatment and tissue acquisition varies. Nevertheless, data retained by histopathological examination of human samples may be closer to the truth than any data collected by in vitro or in vivo experiments.[81]

The results of this study, revealing high inflammatory and proliferative activity, were truly unexpected and appear to be, to some extent, paradoxical to the inhibition of angiogenesis. The question is how to interpret this data in view of promising clinical results related to a decrease in disease activity following intravitreal injection of bevacizumab. There is growing knowledge that inflammatory reactions exert not only proangiogenic activities, but are also involved in vascular regression and angiogenesis inhibition. We assume that a similar process may be reflected in our histopathological results. Our results reveal enhanced expression of the endogenous angiogenesis inhibitor endostatin in these inflammatory active bevacizumab CNVM. Still, our understanding of treatment modalities and combination therapies needs to be further evaluated to implement the optimal treatment

strategies and protocols for neovascular AMD. High inflammatory and proliferative activity as well as enhanced endostatin expression in bevacizumab-treated CNV should be considered when combination therapies with bevacizumab are planned.[11,82,83]

Submitted for Publication: July 19, 2007; final revision received December 17, 2007; accepted December 22, 2007
Author Affiliations: University Eye Hospital, Centre for Ophthalmology, Eberhard-Karls University, Tübingen (Drs Tatar, Yoeruek, Szurman, Bartz-Schmidt, and Grisanti), Department of Pathology, University of Tübingen (Ms Adam), Augenklinik der Staedtischen Kliniken, Frankfurt am Main (Dr Eckardt), and Augenzentrum Recklinghausen, Recklinghausen, Germany (Dr Scharioth); Laboratory of Visual Physiology, National Institute of Sensory Organs, Tokyo, Japan (Dr Shinoda); Algemeen Ziekenhuis Sint Augustinus Hospital, Department Achtersegment, Antwerp, Belgium (Drs Boeyden and Claes); and Department of Ophthalmology, Sacro Cuore Hospital, Negrar, Italy (Dr Pertile). Dr Grisanti is now with the Department of Ophthalmology, University of Lübeck, Lübeck, Germany.
Correspondence: Salvatore Grisanti, MD, Department of Ophthalmology at the University of Lübeck, Ratzeburger Allee 160, 23538 Lübeck, Germany (Salvatore.Grisanti@uk-sh.de).
Author Contributions: Olcay Tatar and Salvatore Grisanti had full access to all of the data in the study and take responsibility for the integrity of the data and the accuracy of the data analysis.
Funding/Support: This work was supported by grants from the Vision 100 Foundation and the Jung Foundation.
Financial Disclosure: None reported.

REFERENCES

1. Hyman L. Epidemiology of eye disease in the elderly. *Eye*. 1987;1(pt 2):330-341.
2. Bressler NM, Bressler SB, Fine SL. Age related macular degeneration. *Surv Ophthalmol*. 1988;32(6):375-413.
3. Guyer DR, Fine SL, Maguire MG, et al. Subfoveal choroidal neovascular membranes in age related macular degeneration: visual prognosis in eyes with relatively good initial visual acuity. *Arch Ophthalmol*. 1986;104(5):702-705.
4. Gragoudas ES, Adamis AP, Cunningham ET Jr, et al; VEGF Inhibition Study in Ocular Neovascularization Clinical Trial Group. Pegaptanib for neovascular age-related macular degeneration. *N Engl J Med*. 2004;351(27):2805-2816.
5. Rosenfeld PJ, Brown DM, Heier JS, et al; MARINA Study Group. Ranibizumab for neovascular age-related macular degeneration. *N Engl J Med*. 2006;355(14):1419-1431.
6. Brown DM, Kaiser PK, Michels M, et al; ANCHOR Study Group. Ranibizumab versus verteporfin for neovascular age-related macular degeneration. *N Engl J Med*. 2006;355(14):1432-1444.
7. Hurwitz H, Fehrenbacher L, Novotny W, et al. Bevacizumab plus irinotecan, fluorouracil, and leucovorin for metastatic colorectal cancer. *N Engl J Med*. 2004;350(23):2335-2342.
8. Moshfeghi AA, Rosenfeld PJ, Puliafito CA, et al. Systemic bevacizumab (Avastin) therapy for neovascular age-related macular degeneration: twenty-four-week results of an uncontrolled open-label clinical study [published online ahead of print October 5, 2006]. *Ophthalmology*. 2006;113(11):2002.e1-2002.e12.
9. Avery RL, Pieramici DJ, Rabena MD, Castellarin AA, Nasir MA, Giust MJ. Intravitreal bevacizumab (Avastin) for neovascular age-related macular degeneration [published online ahead of print February 3, 2006]. *Ophthalmology*. 2006;113(3):363.e5-372.e5.
10. Spaide RF, Laud K, Fine HF, et al. Intravitreal bevacizumab treatment of choroidal neovascularization secondary to age-related macular degeneration. *Retina*. 2006;26(4):383-390.
11. Dhalla MS, Shah GK, Blinder KJ, Ryan EH Jr, Mittra RA, Tewari A. Combined photodynamic therapy with verteporfin and intravitreal bevacizumab for choroidal neovascularization in age-related macular degeneration. *Retina*. 2006;26(9):988-993.
12. Grossniklaus HE, Ling JX, Wallace TM, et al. Macrophage and retinal pigment epithelium expression of angiogenic cytokines in choroidal neovascularization. *Mol Vis*. 2002;8:119-126.
13. Oh H, Takagi H, Takagi C, et al. The potential angiogenic role of macrophages in the formation of choroidal neovascular membranes. *Invest Ophthalmol Vis Sci*. 1999;40(9):1891-1898.
14. Grossniklaus HE, Martinez JA, Brown VB, et al. Immunohistochemical and histochemical properties of surgically excised subretinal neovascular membranes in age-related macular degeneration. *Am J Ophthalmol*. 1992;114(4):464-472.
15. Kim I, Moon SO, Kim SH, Kim HJ, Koh YS, Koh GY. Vascular endothelial growth factor expression of intercellular adhesion molecule 1 (ICAM-1), vascular cell adhesion molecule 1 (VCAM-1), and E-selectin through nuclear factor-kappa B activation in endothelial cells [published online ahead of print December 6, 2000]. *J Biol Chem*. 2001;276(10):7614-7620.
16. Joussen AM, Poulaki V, Qin W, et al. Retinal vascular endothelial growth factor induces intercellular adhesion molecule-1 and endothelial nitric oxide synthase expression and initiates early diabetic retinal leukocytes adhesion in vivo. *Am J Pathol*. 2002;160(2):501-509.
17. Clauss M, Gerlach M, Gerlach H, et al. Vascular permeability factor: a tumor-derived polypeptide that induces endothelial cell and monocyte procoagulant activity, and promotes monocyte migration. *J Exp Med*. 1990;172(6):1535-1545.
18. Lee WS, Jain MK, Arkonac BM, et al. Thy-1, a novel marker for angiogenesis upregulated by inflammatory cytokines. *Circ Res*. 1998;82(8):845-851.
19. Mameros AG, She H, Zambarakji H, et al. Endogenous endostatin inhibits choroidal neovascularization [published online ahead of print May 25, 2007]. *FASEB J*. 2007;21(14):3809-3818.
20. Sunderkötter C, Steinbrink K, Goebeler M, Bhardwaj R, Sorg C. Macrophages and angiogenesis. *J Leukoc Biol*. 1994;55(3):410-422.
21. Ferreras M, Felbor U, Lenhard T, Olsen BR, Delaisse J. Generation and degradation of human endostatin proteins by various proteinases. *FEBS Lett*. 2000;486(3):247-251.
22. Karak AK, Sarkar C, Chumber S, Tandon N. MIB-1 proliferative index in parathyroid adenoma and hyperplasia. *Indian J Med Res*. 1997;105:235-238.
23. Bressler NM, Bressler SB, Childs AL, et al; Submacular Surgery Trials (SST) Research Group. Surgery for hemorrhagic choroidal neovascular lesions of age-related macular degeneration: ophthalmic findings SST report No. 13. *Ophthalmology*. 2004;111(11):1993-2006.
24. Wong D, Stanga P, Briggs M, et al. Case selection in macular relocation surgery for age related macular degeneration. *Br J Ophthalmol*. 2004;88(2):186-190.
25. Gelisken F, Karim-Zoda K, Grisanti S, Bartz-Schmidt KU. Macular translocation with 360 degrees retinotomy for retinal pigment epithelial tear. *Graefes Arch Clin Exp Ophthalmol*. 2005;243(6):619-621.
26. Mruthyunjaya P, Stinnett SS, Toth CA. Change in visual function after macular translocation with 360 degrees retinectomy for neovascular age-related macular degeneration. *Ophthalmology*. 2004;111(9):1715-1724.
27. Aisenbrey S, Lafaut BA, Szurman P, et al. Macular translocation with 360 degrees retinotomy for exudative age-related macular degeneration. *Arch Ophthalmol*. 2002;120(4):451-459.
28. Treatment of Age-Related Macular Degeneration with Photodynamic Therapy (TAP) Study Group. Photodynamic therapy of subfoveal choroidal neovascularization in age-related macular degeneration with verteporfin: one-year results of 2 randomized clinical trials—TAP report 1. *Arch Ophthalmol*. 1999;117(10):1329-1345.
29. Bressler NM, Bressler SB, Childs AL, et al; Treatment of Age-Related Macular Degeneration with Photodynamic Therapy (TAP) Study Group. Photodynamic therapy of subfoveal choroidal neovascularization in age-related macular degeneration with verteporfin: two-year results of 2 randomized clinical trials—TAP report 2. *Arch Ophthalmol*. 2001;119(2):198-207.
30. Avery RL. Regression of retinal and iris neovascularization after intravitreal bevacizumab (Avastin) treatment. *Retina*. 2006;26(3):352-354.
31. Davidorf FH, Mouser JG, Derick RJ. Rapid improvement of rubeosis iridis from a single bevacizumab (Avastin) injection. *Retina*. 2006;26(3):354-356.
32. Spaide RF, Fisher YL. Intravitreal bevacizumab (Avastin) treatment of proliferative diabetic retinopathy complicated by vitreous hemorrhage. *Retina*. 2006;26(3):275-278.
33. Chen E, Park CH. Use of intravitreal bevacizumab as a preoperative adjunct for tractional retinal detachment repair in severe proliferative diabetic retinopathy. *Retina*. 2006;26(6):699-700.
34. Tatar O, Kaiserling E, Adam A, et al. Consequences of verteporfin photodynamic therapy on choroidal neovascular membranes. *Arch Ophthalmol*. 2006;124(6):815-823.

35. Kliffen M, Sharma HS, Mooy CM, Kerkvliet S, de Jong PT. Increased expression of angiogenic growth factors in age-related maculopathy. *Br J Ophthalmol*. 1997; 81(2):154-162.
36. Bhutto IA, McLeod DS, Hasegawa T, et al. Pigment epithelium-derived factor (PEDF) and vascular endothelial growth factor (VEGF) in aged human choroid and eyes with age-related macular degeneration [published online ahead of print July 12, 2005]. *Exp Eye Res*. 2006;82(1):99-110.
37. Marneros AG, Fan J, Yokoyama Y, et al. Vascular endothelial growth factor expression in the retinal pigment epithelium is essential for choriocapillaris development and visual function. *Am J Pathol*. 2005;167(5):1451-1459.
38. Nozaki M, Raisler BJ, Sakurai E, et al. Drusen complement components C3a and C5a promote choroidal neovascularization [published online ahead of print February 1, 2006]. *Proc Natl Acad Sci U S A*. 2006;103(7):2328-2333.
39. Ambati J, Anand A, Fernandez S, et al. An animal model of age-related macular degeneration in senescent Ccl-2- or Ccr-2-deficient mice [published online ahead of print October 19, 2003]. *Nat Med*. 2003;9(11):1390-1397.
40. Barleon B, Sozzani S, Zhou D, Weich HA, Mantovani A, Marme D. Migration of human monocytes in response to vascular endothelial growth factor (VEGF) is mediated via the VEGF receptor flt-1. *Blood*. 1996;87(8):3336-3343.
41. Seregard S, Algvere PV, Berglin L. Immunohistochemical characterization of surgically removed subfoveal fibrovascular membranes. *Graefes Arch Clin Exp Ophthalmol*. 1994;232(6):325-329.
42. Nishimura T, Goodnight R, Prendergast RA, Ryan SJ. Activated macrophages in experimental subretinal neovascularization. *Ophthalmologica*. 1990;200(1): 39-44.
43. Leibovich SJ, Polverini PJ, Shepard HM, et al. Macrophage-induced angiogenesis is mediated by tumour necrosis factor-alpha. *Nature*. 1987;329(6140):630-632.
44. Pavilack MA, Elner VM, Elner SG, Todd RF III, Huber AR. Differential expression of human corneal and perilimbal ICAM-1 by inflammatory cytokines. *Invest Ophthalmol Vis Sci*. 1992;33(3):564-573.
45. Elner SG, Elner VM, Pavilack MA, et al. Modulation and function of intercellular adhesion molecule-1 (CD54) on human retinal pigment epithelial cells. *Lab Invest*. 1992;66(2):200-211.
46. Platts KE, Benson MT, Rennie IG, Sharrard RM, Rees RC. Cytokine modulation of adhesion molecule expression on human retinal pigment epithelial cells. *Invest Ophthalmol Vis Sci*. 1995;36(11):2262-2269.
47. Ferrara N. Vascular endothelial growth factor: basic science and clinical progress. *Endocr Rev*. 2004;25(4):581-611.
48. Sakurai E, Anand A, Ambati BK, van Rooijen N, Ambati J. Macrophage depletion inhibits experimental choroidal neovascularization. *Invest Ophthalmol Vis Sci*. 2003;44(8):3578-3585.
49. Espinosa-Heidmann DG, Suner IJ, Hernandez EP, Monroy D, Csaky KG, Cousins SW. Macrophage depletion diminishes lesion size and severity in experimental choroidal neovascularization. *Invest Ophthalmol Vis Sci*. 2003;44(8):3586-3592.
50. Kwak N, Okamoto N, Wood J, et al. VEGF is major stimulator in model of choroidal neovascularization. *Invest Ophthalmol Vis Sci*. 2000;41(10):3158-3164.
51. Lopez PF, Sippy BD, Lambert HM, et al. Transdifferentiated retinal pigment epithelial cells are immuno-reactive for vascular endothelial growth factor in surgically excised age-related macular degeneration-related choroidal neovascular membranes. *Invest Ophthalmol Vis Sci*. 1996;37(5):855-868.
52. Krzystolik MG, Afshari MA, Adamis AP, et al. Prevention of experimental choroidal neovascularization with intravitreal anti-vascular endothelial growth factor antibody fragment. *Arch Ophthalmol*. 2002;120(3):338-346.
53. Higgins GT, Wang JH, Dockery P, Cleary PE, Redmond HP. Induction of angiogenic cytokine expression in cultured RPE by ingestion of oxidized photoreceptor outer segments. *Invest Ophthalmol Vis Sci*. 2003;44(4):1775-1782.
54. Tezel TH, Bora NS, Kaplan HJ. Pathogenesis of age-related macular degeneration. *Trends Mol Med*. 2004;10(9):417-420.
55. Bora NS, Kaliappan S, Jha P, et al. CD59, a complement regulatory protein, controls choroidal neovascularization in a mouse model of wet-type age-related macular degeneration. *J Immunol*. 2007;178(3):1783-1790.
56. Sakurai E, Taguchi H, Anand A, et al. Targeted disruption of the CD18 or ICAM-1 gene inhibits choroidal neovascularization. *Invest Ophthalmol Vis Sci*. 2003; 44(6):2743-2749.
57. Shi X, Semkova I, Muther PS, Dell S, Kociok N, Joussen AM. Inhibition of TNF-alpha reduces laser-induced choroidal neovascularization [published online ahead of print September 7, 2006]. *Exp Eye Res*. 2006;83(6):1325-1334.
58. Sakurai E, Nozaki M, Raisler BJ, et al. Inhibition of choroidal neovascularization by VEGF—a blockade is mediated via Ccl-2 suppression [ARVO E-abstract]. *Invest Ophthalmol Vis Sci*. 2005;46:E-abstract 3027.
59. Tsuchihashi S, Ke B, Kaldas F, et al. Vascular endothelial growth factor antagonist modulates leukocyte trafficking and protects mouse livers against ischemia/reperfusion injury. *Am J Pathol*. 2006;168(2):695-705.
60. Shahar J, Avery RL, Heilweil G, et al. Electrophysiologic and retinal penetration studies following intravitreal injection of bevacizumab (Avastin). *Retina*. 2006; 26(3):262-269.
61. Alon T, Hemo I, Itin A, Pe'er J, Stone J, Keshet E. Vascular endothelial growth factor acts as a survival factor for newly formed retinal vessels and has implications for retinopathy of prematurity. *Nat Med*. 1995;1(10):1024-1028.
62. Baffert F, Le T, Sennino B, et al. Cellular changes in normal blood capillaries undergoing regression after inhibition of VEGF signaling [published online ahead of print September 19, 2005]. *Am J Physiol Heart Circ Physiol*. 2006;290(2): H547-H559.
63. Kamba T, Tam BY, Hashizume H, et al. VEGF-dependent plasticity of fenestrated capillaries in the normal adult microvasculature [published online ahead of print September 19, 2005]. *Am J Physiol Heart Circ Physiol*. 2006;290(2):H560-H576.
64. Meeson AP, Argilla M, Ko K, Witte L, Lang RA. VEGF deprivation-induced apoptosis is a component of programmed capillary regression. *Development*. 1999; 126(7):1407-1415.
65. Lobov IB, Rao S, Carroll TJ, et al. WNT7b mediates macrophage-induced programmed cell death in patterning of the vasculature. *Nature*. 2005;437(7057): 417-421.
66. Chavakis T, Cines DB, Rhee JS, et al. Regulation of neovascularization by human neutrophil peptides (alpha-defensins): a link between inflammation and angiogenesis [published online ahead of print June 19, 2004]. *FASEB J*. 2004; 18(11):1306-1308.
67. Lang RA. Apoptosis in mammalian eye development: lens morphogenesis, vascular regression and immune privilege. *Cell Death Differ*. 1997;4(1):12-20.
68. Diez-Roux G, Argilla M, Makarenkova H, Ko K, Lang RA. Macrophages kill capillary cells in G1 phase of the cell cycle during programmed vascular regression. *Development*. 1999;126(10):2141-2147.
69. Diez-Roux G, Lang RA. Macrophages induce apoptosis in normal cells in vivo. *Development*. 1997;124(18):3633-3638.
70. Apte RS, Richter J, Herndon J, Ferguson TA. Macrophages inhibit neovascularization in a murine model of age-related macular degeneration. *PLoS Med*. 2006; 3(8):e310.
71. Bhutto IA, Kim SY, McLeod DS, et al. Localization of collagen XVIII and the endostatin portion of collagen XVIII in aged human control eyes and eyes with age-related macular degeneration. *Invest Ophthalmol Vis Sci*. 2004;45(5):1544-1552.
72. Li W, He Z, Li Y, Yanoff M. Vascular endothelial growth factor regulates both apoptosis and angiogenesis of choriocapillaris endothelial cells. *Microvasc Res*. 2000;59(2):286-289.
73. Leung DW, Cachianes G, Kuang WJ, Goeddel DV, Ferrara N. Vascular endothelial growth factor is a secreted angiogenic mitogen. *Science*. 1989;246(4935): 1306-1309.
74. Guerrin M, Moukadiri H, Chollet P, et al. Vasculotropin/vascular endothelial growth factor is an autocrine growth factor for human retinal pigment epithelial cells cultured in vitro. *J Cell Physiol*. 1995;164(2):385-394.
75. Hoffmann S, Masood R, Zhang Y, et al. Selective killing of RPE with a vascular endothelial growth factor chimeric toxin. *Invest Ophthalmol Vis Sci*. 2000;41 (8):2389-2393.
76. Zubilewicz A, Hecquet C, Jeanny JC, Soubrane G, Courtois Y, Mascarelli F. Two distinct signaling pathways are involved in FGF2-stimulated proliferation of choriocapillary endothelial cells: a comparative study with VEGF. *Oncogene*. 2001; 20(12):1403-1413.
77. Geisen P, McColm JR, Hartnett ME. Choroidal endothelial cells transmigrate across the retinal pigment epithelium but do not proliferate in response to soluble vascular endothelial growth factor. *Exp Eye Res*. 2006;82(4):608-619.
78. Peters S, Julien S, Heiduschka P, et al; Tuebingen Bevacizumab Study Group. Anti-permeability and anti-proliferative effects of standard and frozen bevacizumab on choroidal endothelial cells [published online ahead of print December 19, 2006]. *Br J Ophthalmol*. 2007;91(6):827-831.
79. Spitzer MS, Wallenfels-Thilo B, Sierra A, et al; Tuebingen Bevacizumab Study Group. Antiproliferative and cytotoxic properties of bevacizumab on different ocular cells [published online ahead of print May 24, 2006]. *Br J Ophthalmol*. 2006;90(10):1316-1321.
80. Tatar O, Shinoda K, Adam A, et al. Expression of endostatin in human choroidal neovascular membranes secondary to age-related macular degeneration [published online ahead of print April 11, 2006]. *Exp Eye Res*. 2006;83(2):329-338.
81. Arroyo JG. Towards a rational approach to combination therapy for neovascular age-related macular degeneration. *Br J Ophthalmol*. 2007;91(2):130-131.
82. Ahmadieh H, Taei R, Soheilian M, et al. Single-session photodynamic therapy combined with intravitreal bevacizumab and triamcinolone for neovascular age-related macular degeneration. *BMC Ophthalmol*. 2007;7:10.
83. Augustin AJ, Puls S, Offermann I. Triple therapy for choroidal neovascularization due to age-related macular degeneration: verteporfin PDT, bevacizumab, and dexamethasone. *Retina*. 2007;27(2):133-140.

ORIGINAL ARTICLE

Angiotensin II Type 1 Receptor Signaling Contributes to Synaptophysin Degradation and Neuronal Dysfunction in the Diabetic Retina

Toshihide Kurihara,[1,2,3] Yoko Ozawa,[1,2,3] Norihiro Nagai,[1,2] Kei Shinoda,[4] Kousuke Noda,[1,2] Yutaka Imamura,[5] Kazuo Tsubota,[2] Hideyuki Okano,[3] Yuichi Oike,[6] and Susumu Ishida[1,2]

OBJECTIVE—Pathogenic mechanisms underlying diabetes-induced retinal dysfunction are not fully understood. The aim of the present study was to show the relationship of the renin-angiotensin system (RAS) with the synaptic vesicle protein synaptophysin and neuronal activity in the diabetic retina.

RESEARCH DESIGN AND METHODS—C57BL/6 mice with streptozotocin-induced diabetes were treated with the angiotensin II type 1 receptor (AT1R) blocker telimsartan or valsartan, and retinal function was analyzed by electroretinography. Retinal production of the RAS components and phosphorylation of ERK (extracellular-signal regulated kinase) were examined by immunoblotting. Retinal mRNA and protein levels of synaptophysin were measured by quantitative RT-PCR and immunoblot analyses, respectively. In vitro, synaptophysin levels were also evaluated using angiotensin II–stimulated PC12D neuronal cells cultured with or without the inhibition of ERK signaling or the ubiquitin-proteasome system (UPS).

RESULTS—Induction of diabetes led to a significant increase in retinal production of angiotensin II and AT1R together with ERK activation in the downstream of AT1R. AT1R blockade significantly reversed diabetes-induced electroretinography changes and reduction of synaptophysin protein, but not mRNA, levels in the diabetic retina. In agreement with the AT1R-mediated post-transcriptional downregulation of synaptophysin in vivo, in vitro application of angiotensin II to PC12D neuronal cells caused the UPS-mediated degradation of synaptophysin protein via AT1R, which proved to be induced by ERK activation.

CONCLUSIONS—These data indicate the first molecular evidence of the RAS-induced synaptophysin degradation and neuronal dysfunction in the diabetic retina, suggesting the possibility of the AT1R blockade as a novel neuroprotective treatment for diabetic retinopathy. ***Diabetes* 57:2191–2198, 2008**

From the [1]Laboratory of Retinal Cell Biology, Keio University School of Medicine, Tokyo, Japan; the [2]Department of Ophthalmology, Keio University School of Medicine, Tokyo, Japan; the [3]Department of Physiology, Keio University School of Medicine, Tokyo, Japan; the [4]Department of Ophthalmology, Oita University Faculty of Medicine, Hasama-machi, Yufu-shi, Oita, Japan; the [5]Inaida Laboratory for Anti-Aging Medicine, Keio University School of Medicine, Tokyo, Japan; the [6]Department of Molecular Genetics, Graduate School of Medical Sciences, Kumamoto University, Kumamoto, Japan.

Corresponding author: Susumu Ishida, ishidasu@sc.itc.keio.ac.jp.

Received 11 September 2007 and accepted 12 May 2008.
Published ahead of print at http://diabetes.diabetesjournals.org on 16 May 2008. DOI: 10.2337/db07-1281.
T.K. and Y.O. contributed equally to this work.

Diabetic retinopathy is a vision-threatening disease with neurodegenerative change due to chronically progressive microangiopathy. The earliest functional disruption clinically detectable is changes in oscillatory potentials (OPs) measured by electroretinography (ERG) (1,2). The cellular source of OPs is regarded as retinal neurons with synapse formation in the inner retina, including bipolar and amacrine cells (3). At present, there is no established neuroprotective treatment for diabetic retinopathy, since molecular mechanisms underlying diabetes-induced retinal neuronal damage remain unclear.

We have recently demonstrated that angiotensin II type 1 receptor (AT1R) signaling contributes to diabetes-induced retinal inflammation such as leukocyte adhesion to the retinal vasculature (4). Angiotensin II functions as a proinflammatory factor to induce the activation of nuclear factor-κB pathway in microvascular endothelial cells (4). Angiotensin II is a final product of the renin-angiotensin system (RAS) produced from angiotensinogen through enzymatic cascade reactions, and the RAS components required for the generation of angiotensin II are reported to exist in the eye (5–7). Indeed, human surgical samples from eyes with diabetic retinopathy showed a significant increase in angiotensin II levels (8–10). Increasing evidence has suggested the contribution of the RAS to diabetes-induced retinal vascular complications including leukocyte adhesion (4), hyperpermeability (11), and impaired blood flow (12); however, little is known about the pathogenesis of angiotensin II–mediated neuronal dysfunction in the diabetic retina. Although AT1R blockade led to amelioration of hypertension-induced retinal dysfunction that was exacerbated with diabetes (13), no data have been reported that show the direct effect of AT1R signaling on diabetes-induced retinal dysfunction together with underlying molecular mechanisms.

Recently, we revealed the coexpression of AT1R and the synaptic protein synaptophysin in the inner retinal neurons (14), consistent with several previous reports showing synaptic expression of AT1R in the brain (15–18). Synaptophysin, the major synaptic vesicle protein, is a marker of synapses reported to be reduced in the postmortem brains affected by several neurodegenerative diseases (19). Considering that OPs in ERG are originated from inner retinal neurons bearing AT1R, we hypothesize that angiotensin II directly induces synaptophysin dysregulation and visual functional damage represented by ERG changes. In the present article, we report the first evidence showing that AT1R signaling contributes to diabetes-induced retinal dysfunction and

TABLE 1
Systemic data

	Nondiabetes	Diabetes		
		Vehicle	Telmisartan	Valsartan
n	17	17	18	18
Body weight (g)	26.0 ± 1.3	24.2 ± 1.3†	24.8 ± 1.1*	24.3 ± 1.2†
Blood glucose (mg/dl)	156 ± 22	544 ± 64†	539 ± 81†	516 ± 96†

*$P < 0.05$, †$P < 0.01$ vs. nondiabetes.

synaptophysin downregulation together with underlying molecular mechanisms.

RESEARCH DESIGN AND METHODS

Induction of diabetes. C57BL/6 mice (Clea, Tokyo, Japan) at the age of 6 weeks were used in diabetes induction. All animal experiments were conducted in accordance with the ARVO (Association for Research in Vision and Ophthalmology) Statement for the Use of Animals in Ophthalmic and Vision Research. Animals received intraperitoneal injections of streptozotocin (Sigma, St. Louis, MO) at the dose of 60 mg/kg body weight for 3 days. Blood glucose concentrations were measured from the tail vein using Medisafe mini GR-102 (Terumo, Tokyo, Japan). Development of diabetes was defined by blood glucose >250 mg/dl 7 days after the first injection of streptozotocin.

AT1R blockade in vivo. Mice were intraperitoneally injected with the AT1R blocker (ARB) telmisartan or valsartan (U.S. Pharmacopeia, Rockville, MD) at the dose of 5 or 10 mg/kg body weight, respectively, or vehicle (0.25% DMSO in PBS). The ARB treatment started 22 days after the first injection of streptozotocin for 6 consecutive days and continued until the end of the study (4-week diabetes at evaluation). The doses used in each ARB group were determined according to our previous study on diabetes-induced retinal inflammation (4). Telmisartan was a kind gift of Boehringer Ingelheim (Ingelheim, Germany).

ERG analyses. Animals were dark-adapted for 12 h and prepared under dim red illumination. Mice were anesthetized with pentobarbital sodium at the dose of 70 mg/kg body weight and placed on a heating pad that maintained their body temperature at 35–36°C throughout the experiments. The pupils were dilated with a mixed solution of 0.5% tropicamide and 0.5% phenylephrine (Mydrin-P; Santen, Osaka, Japan). The ground electrode was a subcutaneous needle in the tail, and the reference electrode was placed subcutaneously between the eyes. The active contact lens electrodes (Mayo, Inazawa, Japan) were placed on the cornea. Recordings were performed with PowerLab system 2/25 (AD Instruments, New South Wales, Australia). Responses were differentially amplified at the gain of 1,000 times using an AC (alternate current)-coupled bioamplifier ML132 (AD Instruments) and filtered through a bandpass filter ranging from 0.3 to 500 Hz to yield a- and b-waves. OPs were simultaneously recorded using a high-pass filter set to 100 Hz, so that an overall bandpass ranging from 100 to 500 Hz was achieved. Light pulses of 800 cd-s/m^2 were delivered via Ganzfeld System SG-2002 (LKC Technologies; Gaithersburg, MD). The amplitude and implicit time of the a- and b-waves and OPs were measured and compared among age-matched nondiabetic controls and 4-week diabetic animals treated with vehicle, telmisartan, or valsartan.

In vitro assays. The neuronal cell line PC12D cells were cultured in Dulbecco's modified Eagle's medium (DMEM; Invitrogen, Carlsbad, CA) supplemented with 10% fetal bovine serum and 10% horse serum (Medical & Biological Laboratories, Nagoya, Japan). Cells were incubated with 50 μg/μl of nerve growth factor (Millipore, Billerica, MA) for differentiation to neurons for 2 days. The neuronal cells were applied with the ARB telmisartan (10 μmol/l) or valsartan (25 μmol/l), the proteasome inhibitor MG132 or lactacystin (20 μmol/l for both; Calbiochem, San Diego, CA), the lysosome inhibitor E64 (50 μmol/l; Sigma), the extracellular signal–regulated kinase (ERK) kinase inhibitor U0126 (10 μmol/l; Cell Signaling Technology, Beverly, MA) or PD98059 (10 μmol/l; Calbiochem), the phosphatidylinositol 3-kinase inhibitor LY294002 (20 μmol/l; Calbiochem) or wortmannin (100 nmol/l; Sigma), the Janus kinase inhibitor AG490 (1, 10, or 100 μmol/l; Calbiochem), or vehicle. After 5 min, the pretreated cells were subsequently stimulated with 100 nmol/l angiotensin II for 30 min. Immediately after the exposure to angiotensin II, the neuronal cells were subjected to quantitative RT-PCR and immunoprecipitation for synaptophysin and to immunoblot analyses for synaptophysin and phosphorylated forms of ERK1/2 (p44/p42), Akt (protein kinase B), and signal transducer and activator of transcription (STAT)-3.

AT1R and ERK1/2 knockdown by RNA interference. Transfections were performed using Lipofectamine 2000 (Invitrogen) and the SureSilencing short hairpin RNA (shRNA) kit (SuperArray Bioscience, Frederick, MD) according to the manufacturers' instructions. Briefly, 4 μg Rat Agtr1a (AT1R), Rat Mapk3 (ERK1), and Rat Mapk1 (ERK2) or control shRNA was incubated with 10 μl of the transfection reagent in 500 μl serum-free medium for 20 min to facilitate complex formation. The resulting mixture was added to PC12D cells cultured in a six-well plate with 2 ml medium for 48 h before differentiation.

Quantitative RT-PCR analyses for synaptophysin. Animals were killed with an overdose of anesthesia. The eyes were immediately enucleated and the retina was carefully isolated. Total RNA was extracted from the retinas or PC12D cells using an extraction reagent (TRIzol; Invitrogen), and cDNA was synthesized with SuperScript III reverse transcriptase (Invitrogen). Real-time PCR was performed using MX3000 (Stratagene, La Jolla, CA) with PCR primers for synaptophysin designed by TaqMan Gene Expression Assays (Applied Biosystems, Foster, CA). The mRNA levels were normalized to β-actin as an internal control.

Immunoblot analyses for angiotensin II, AT1R, synaptophysin, and phosphorylated forms of ERK, Akt, and STAT3. The isolated retinas or PC12D cells were placed into lysis buffer (10 mmol/l Tris-HCl [pH 7.6], 100 mmol/l NaCl, 1 mmol/l EDTA, 1% Triton X-100, protease inhibitors). Each sample was separated with SDS-PAGE and electroblotted to polyvinylidene fluoride (PVDF) membranes (Millipore, Bedford, MA). After nonspecific binding was blocked with 4% skim milk, the membranes were incubated at 4°C overnight with a rabbit polyclonal antibody against angiotensin II, AT1R (1:200, 1:100, respectively; Santa Cruz Biotechnology, Santa Cruz, CA), or phosphorylated forms of ERK, Akt, or STAT3 (1:1,000, 1:500, or 1:1,000, respectively; Cell Signaling Technology) or a mouse monoclonal antibody against synaptophysin (1:500; Sigma) or α-tubulin (1:2,000; Sigma). The membranes were then incubated with a horseradish peroxidase–conjugated goat antibody against rabbit or mouse immunoglobulins or with a biotinylated secondary antibody followed by avidin-biotin horseradish peroxidase complexes (Vectastain Elite ABC Kit; Vector, Burlingame, CA). The signals were visualized with chemiluminescence (ECL Blotting Analysis System; Amersham, Arlington Heights, IL), measured by ImageJ software (National Institutes of Health, Bethesda, MD) and normalized to α-tubulin.

Ubiquitination assays. PC12D cells were transfected with a hemagglutinin-ubiquitin plasmid (provided by Keiji Tanaka, the Tokyo Metropolitan Institute of Medical Science, Tokyo, Japan) as described above at the time of differentiation. Forty-five hours after transfection, the cells were incubated for 3 h with 20 μmol/l MG132. The transfected cells were then pretreated with telmisartan, valsartan, or vehicle and followed by stimulation with angiotensin II as described above. The stimulated cells were placed into the lysis buffer, and the cell lysate was applied with a rabbit polyclonal antibody against synaptophysin (1:25; Sigma). After rocking at 4°C for 1 h, the lysate treated with anti-synaptophysin antibodies were then added with protein G-sepharose beads (Sigma) and incubated overnight at 4°C. After washes of nonspecific binding to beads, the bound protein was solubilized in sample buffer, loaded on an SDS-PAGE, and processed for immunoblotting with a rat monoclonal antibody against hemagglutinin (1:500; Roche Applied Science, Mannheim, Germany) to detect multi-ubiquitinated synaptophysin and with a mouse monoclonal antibody against synaptophysin (1:500; Sigma) to confirm the equal amount of synaptophysin protein applied in each lane.

Statistical analysis. All results were expressed as means ± SD. The values were processed for statistical analyses (one-way ANOVA with Tukey's post hoc test), and differences were considered statistically significant at $P < 0.05$.

RESULTS

Diabetes-induced retinal production of angiotensin II and AT1R led to ERK activation. Mice with streptozotocin-induced diabetes showed a significant ($P < 0.05$) decrease in body weight and a significant ($P < 0.01$) increase in blood glucose, compared with age-matched nondiabetic controls (Table 1). Treatment with telmisar-

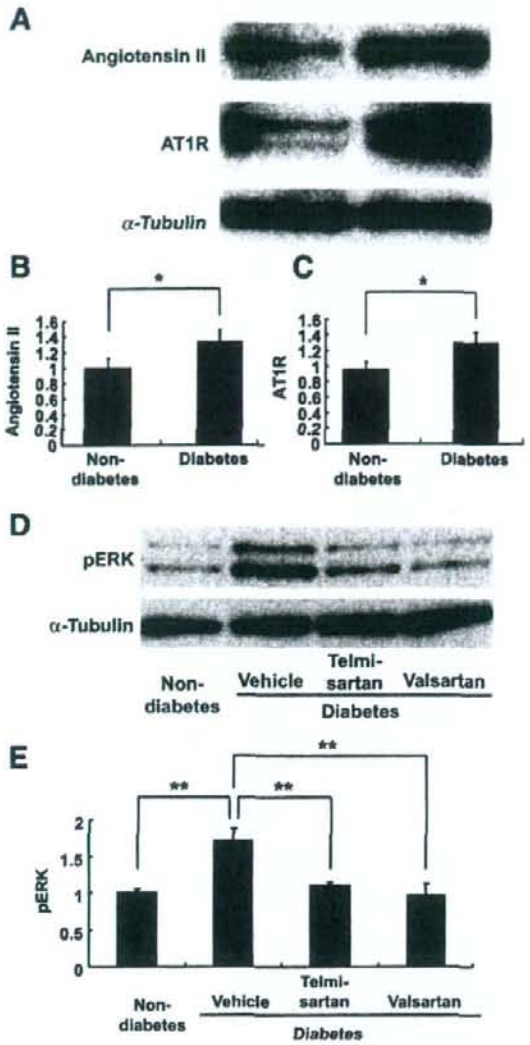

FIG. 1. Diabetes-induced retinal production of angiotensin II and AT1R led to ERK activation. Immunoblot analyses showing the production of the RAS components (*A–C*) and ERK activation in the diabetic retina (*D* and *E*). Retinal levels of angiotensin II and AT1R were significantly higher in 4-week diabetic than in nondiabetic mice (*A–C*). ERK phosphorylation, elevated in 4-week diabetic mice, was significantly attenuated by AT1R blockade with telmisartan or valsartan (*D* and *E*). n = 4 for all. $^*P < 0.05$.

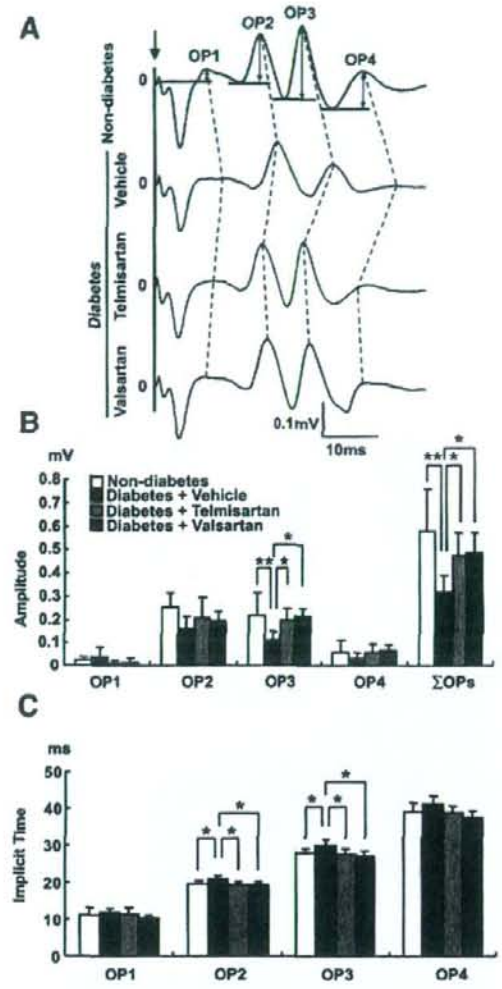

FIG. 2. Diabetes-induced visual dysfunction was suppressed by AT1R blockade. *A*: Representative wave responses from an individual mouse in each group to one flash. *A* and *B*: ERG analyses showing that AT1R blockade with telmisartan or valsartan significantly reversed the reduction of OP3 and total OPs (ΣOPs) amplitude in 4-week diabetic mice. Similarly, the implicit time of OP2–3, prolonged in 4-week diabetic mice, was significantly recovered by AT1R blockade (*A* and *C*). n = 7–9. $^*P < 0.05$, $^{**}P < 0.01$.

tan or valsartan of 4-week diabetic mice did not significantly ($P > 0.05$) change these metabolic parameters (Table 1). The retinas from 4-week diabetic mice were subjected to immunoblot analyses to detect the production of the RAS components and its downstream ERK activation (Fig. 1). Retinal levels of angiotensin II and its receptor AT1R were significantly ($P < 0.01$) higher in 4-week diabetic than in nondiabetic animals (Fig. 1*A–C*). Consistently, ERK phosphorylation, enhanced in 4-week diabetic mice ($P < 0.01$), was significantly ($P < 0.01$) attenuated by AT1R blockade with telmisartan or valsartan to the level equivalent with that in nondiabetic mice (Fig. 1*D* and *E*). In contrast, AT1R blockade did not attenuate the baseline level of retinal pERK in nondiabetic mice (data not shown).

Diabetes-induced visual dysfunction was suppressed by AT1R blockade. To determine the effect of the RAS activation in the diabetic retina (Fig. 1) on visual function, we performed ERG analyses (Fig. 2). OP changes including the reduced amplitude and prolonged implicit time are known to occur in the early stage of murine and human diabetic retinopathy (1,2,20,21). There was no remarkable difference in a- or b-wave among nondiabetes and 4-week diabetes treated with vehicle, telimsartan, and valsartan (data not shown). Importantly, AT1R blockade with telmisartan or valsartan significantly reversed the reduction of

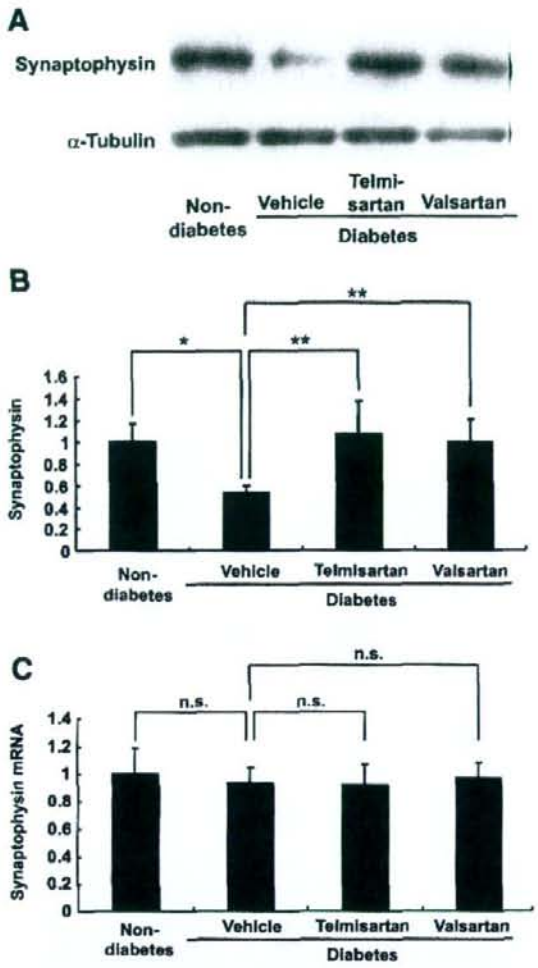

FIG. 3. Posttranscriptional reduction of synaptophysin in the diabetic retina was reversed by AT1R blockade. The retinal levels of synaptophysin protein, reduced by inducing diabetes, were significantly reversed in 4-week diabetic mice by AT1R blockade with telmisartan or valsartan (*A* and *B*). In contrast, mRNA levels of synaptophysin were unaltered in 4-week diabetic mice treated with vehicle, telmisartan, or valsartan compared with age-matched nondiabetic control animals (*C*). $n = 4–8$. *$P < 0.05$, **$P < 0.01$.

OP3 and total OPs (ΣOPs) amplitude ($P < 0.05$ for both) in 4-week diabetic mice (Fig. 2*A* and *B*). Similarly, the implicit time of OP2 and OP3, prolonged in 4-week diabetic mice, was significantly ($P < 0.05$ for both) recovered by AT1R blockade to the normal level (Fig. 2*A* and *C*). In contrast, AT1R blockade did not alter normal ERG waves in nondiabetic mice (data not shown).

Posttranscriptional reduction of synaptophysin in the diabetic retina was reversed by AT1R blockade. To investigate the molecular mechanisms underlying the AT1R-mediated impairment of ERG responses (Fig. 2), we analyzed the regulation of the synaptic vesicle protein synaptophysin (Fig. 3), which is abundantly expressed in the inner retinal neurons (14), the cellular source of OPs (1,3,22,23). Synaptophysin is indispensable for several presynaptic functions, including the release of neurotransmitters (24). The retinal levels of synaptophysin protein, reduced by inducing diabetes, were significantly ($P < 0.01$) reversed in 4-week diabetic mice by AT1R blockade with telmisartan or valsartan (Fig. 3*A* and *B*). In contrast, mRNA levels of synaptophysin were unaltered in 4-week diabetic mice treated with vehicle, telimsartan, or valsartan, compared with those in age-matched nondiabetic controls (Fig. 3*C*). The discrepancy between the protein and mRNA levels indicated that the AT1R-mediated decline of synaptophysin in the diabetic retina was posttranscriptionally regulated. In contrast, AT1R blockade did not affect the physiologic level of synatophysin mRNA or protein in the nondiabetic retina (data not shown).

AT1R-mediated posttranscriptional reduction of synaptophysin was regulated by the ubiquitin-proteasome system in neuronal cells. To elucidate the molecular mechanisms involving the AT1R-mediated posttranscriptional decrease in synaptophysin in the diabetic retina (Fig. 3), we used the in vitro culture system with PC12D neuronal cells stimulated with angiotensin II (Fig. 4). In agreement with the in vivo data (Fig. 3), in vitro application with angiotensin II significantly ($P < 0.01$) reduced synaptophysin protein (Fig. 4*A* and *B*), but not mRNA (Fig. 4*C*), levels in a posttranscriptional manner, which were significantly ($P < 0.05$ for all) reversed by AT1R blockade with telmisartan, valsartan, or shRNA for AT1R knockdown (Fig. 4*A*, *B*, and *D–F*). Because synaptic vesicle proteins including synaptophysin have recently proven to be physiologically degraded by the UPS for the maintenance of synaptic plasticity (25–27), we examined the involvement of the ubiquitin-proteasome system (UPS) (Fig. 4*G–I*) with AT1R-mediated posttranscriptional decrease in synaptophysin protein (Fig. 4*A–F*). Multi-ubiquitinated synaptophysin as a high–molecular weight smear, enhanced by stimulation with angiotensin II, was substantially attenuated by AT1R blockade with telmisartan or valsartan (Fig. 4*G*). Application with the proteasome inhibitor MG132 or lactacystin, but not the lysosome inhibitor E64, led to significant ($P < 0.05$) suppression of angiotensin II–induced degradation of synaptophysin (Fig. 4*H* and *I*). In contrast, the baseline levels of synaptophysin in PC12D cells not stimulated with angiotensin II were unaffected with these inhibitors (data not shown).

AT1R-mediated ERK activation was required for synaptophysin degradation in neuronal cells. Because ERK was activated in the downstream of AT1R signaling in the diabetic retina (Fig. 1), we examined the involvement of ERK activation (Fig. 5) with AT1R-mediated degradation of synaptophysin in the neuronal cells (Fig. 4). Consistent with AT1R-mediated ERK activation in the diabetic retina (Fig. 1), angiotensin II administration induced the phosphorylation of ERK in the neuronal cells, which was significantly ($P < 0.05$) inhibited by AT1R blockade with telmisartan or valsartan (Fig. 5*A* and *B*). Inhibition of ERK activation with U0126, PD98059, or shRNA for ERK1/2 knockdown led to significant ($P < 0.05$ for all) suppression of angiotensin II–induced degradation of synaptophysin (Fig. 5*C–H*). In addition to ERK signaling, phosphatidylinositol 3-kinase/Akt and Janus kinase/STAT pathways are known to be in the downstream of AT1R. In the neuronal cells, angiotensin II treatment also increased the phosphorylated forms of Akt and STAT3 (data not shown). In contrast to ERK involvement (Fig. 5*C–H*), however, the phosphatidylinositol 3-kinase inhibitor wortmannin or LY294002 or the Janus kinase inhibitor AG490 did not

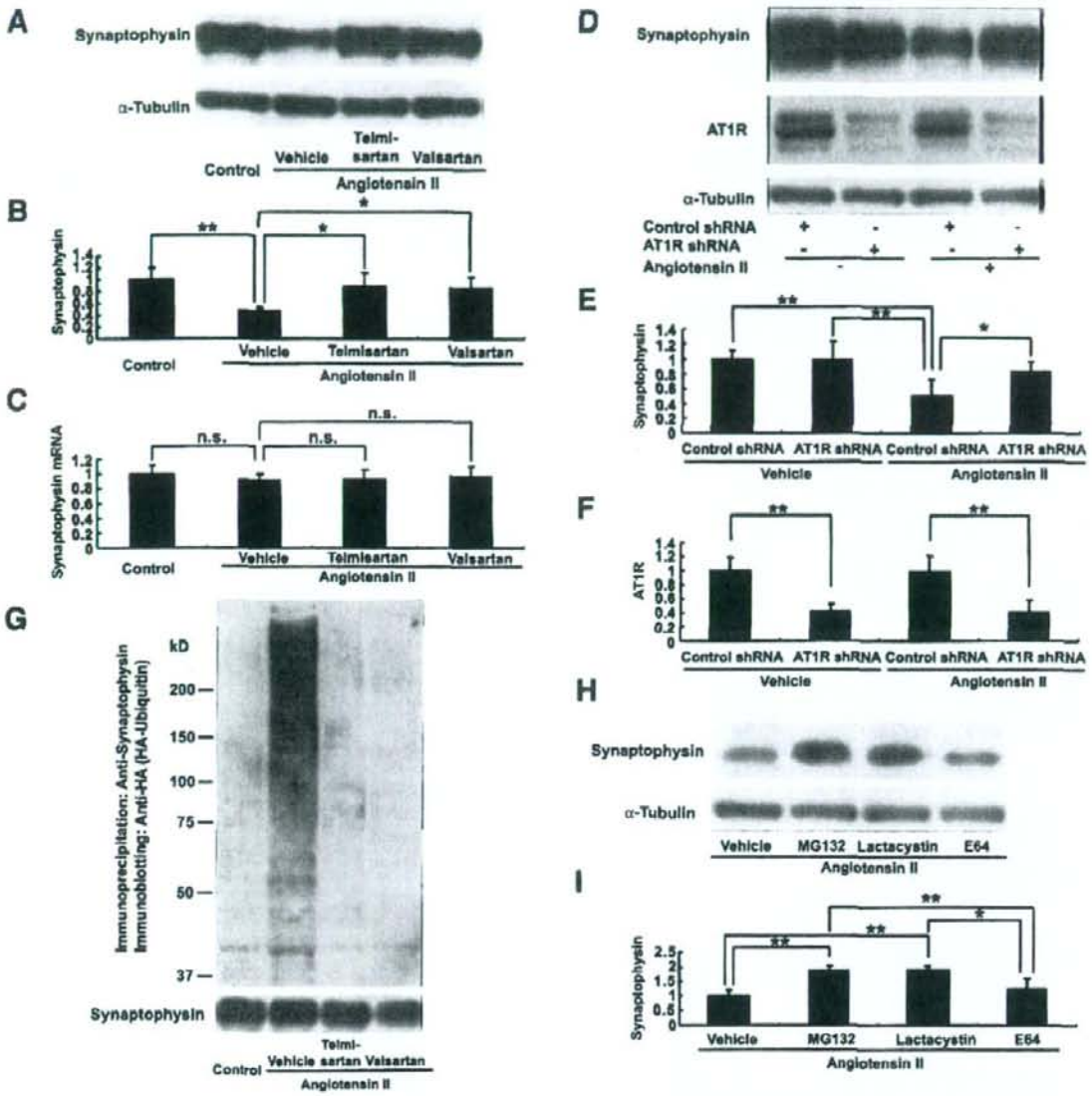

FIG. 4. AT1R-mediated posttranscriptional reduction of synaptophysin was regulated by the UPS in neuronal cells. In vitro application with angiotensin II significantly reduced synaptophysin protein (*A* and *B*), but not mRNA (*C*), levels in a posttranscriptional manner, which were significantly reversed by AT1R blockade with telmisartan or valsartan. The data with the pharmacologic AT1R blockade (*A–C*) were reproduced via shRNA for AT1R knockdown (*D–F*). Multi-ubiquitinated synaptophysin as a high-molecular weight smear, enhanced by stimulation with angiotensin II, was substantially attenuated by AT1R blockade (*G*). Application with the proteasome inhibitor MG132 or lactacystin, but not the lysosome inhibitor E64, led to significant suppression of angiotensin II–induced degradation of synaptophysin (*H* and *I*). $n = 4–6$. $^{*}P < 0.05$, $^{**}P < 0.01$.

reverse angiotensin II–induced degradation of synaptophysin in vitro (data not shown).

DISCUSSION

The present study reveals, for the first time to our knowledge, several important findings concerning the relationship of the RAS with diabetes-related neuronal damage in vivo and in vitro. In the diabetic retina, the RAS components angiotensin II and AT1R were upregulated together with AT1R's downstream ERK activation (Fig. 1). AT1R blockade with telmisartan or valsartan significantly reversed diabetes-induced OP changes measured by ERG (Fig. 2), known functional abnormalities in human diabetic retinopathy. Moreover, AT1R signaling caused a posttranscriptional decrease in the synaptic vesicle protein synaptophysin in the diabetic retina, which was rescued by the ARB application to diabetic mice (Fig. 3). The protein, but not mRNA, reduction of synaptophysin in neuronal cells was shown to depend on the UPS, which was enhanced via AT1R signaling (Fig. 4). Angiotensin II–induced neuronal ERK

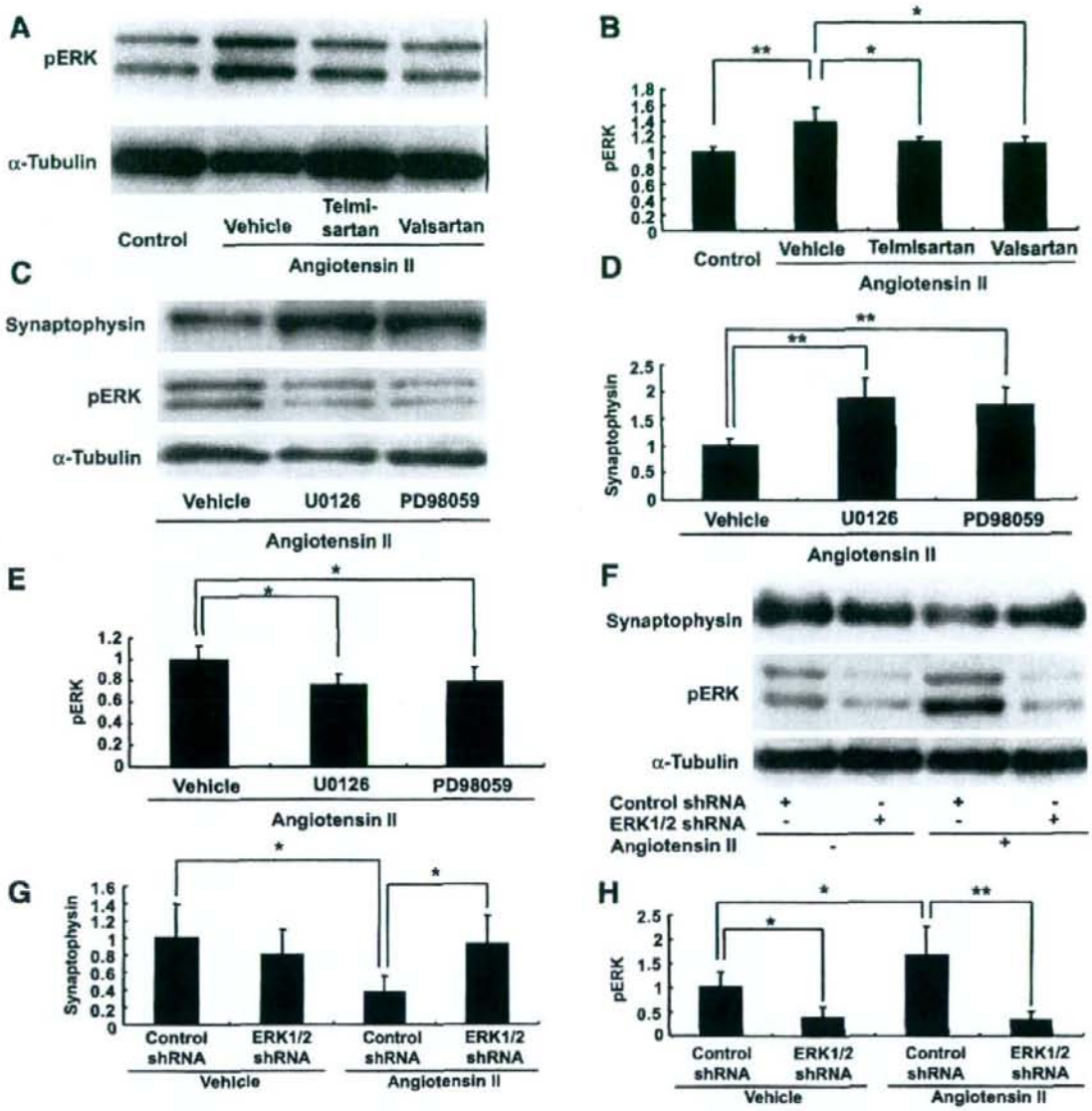

FIG. 5. AT1R-mediated ERK activation was required for synaptophysin degradation in neuronal cells. Angiotensin II administration induced the phosphorylation of ERK in the neuronal cells, which was significantly inhibited by AT1R blockade with telmisartan or valsartan (*A* and *B*). Inhibition of ERK activation with U0126 or PD98059 led to significant suppression of angiotensin II–induced decline of synaptophysin (*C–E*). The data with the pharmacologic ERK inhibition (*C–E*) were reproduced via shRNA for ERK1/2 knockdown (*F–H*). $n = 4–6$. *$P < 0.05$, **$P < 0.01$.

activation, also observed in the diabetic retina (Fig. 1), resulted in the degradation of synaptophysin protein in vitro (Fig. 5). The use of two different ARBs throughout the experiments confirmed that the suppression of diabetes-induced retinal dysfunction and synaptophysin degradation is a class effect for ARBs. Additionally, our in vitro results were further confirmed via gene-specific shRNA knockdown technique for AT1R and ERK.

In the diabetic retina, the production of angiotensin II and AT1R was upregulated, leading to ERK activation in the downstream of AT1R signaling (Fig. 1). Since ERK is known to be one of AT1R's signaling pathways, the present data are compatible with clinical (5,7,28,29) and experimental (4) studies showing increased angiotensin II generation in the diabetic eye. The cellular source of angiotensin II was shown to be retinal glial cells by immunohistochemistry for human postmortem eyes (30). In the liver and kidney as well (31–33), diabetes-induced activation of the RAS causes elevated concentration of tissue angiotensin II. The tissue RAS activation in diabetes is explained in part by the findings that in vitro stimulation with high glucose enhanced the transcriptional activity of angiotensinogen gene encoding a precursor protein for angiotensin I and II (34,35).

Our ERG analyses demonstrated the reduced amplitude and prolonged implicit time of OPs in diabetic mice, in accordance with clinical and experimental data on attenuated OP changes in early diabetes (1,2,29). Importantly, AT1R blockade significantly improved these functional parameters in the diabetic retina to the normal levels observed in nondiabetic controls (Fig. 2). Reasonably, the present ERG findings, in concert with our recent data on AT1R expression in the inner retinal neurons (14), the cellular origins of OPs, suggest that the functional recovery of the diabetic inner retina was attributable in part to the direct effect of AT1R blockade on the inner retinal neurons.

Several previous studies on neuronal damage in the diabetic retina showed the cellular changes including the apoptosis of ganglion and amacrine cells and the activation of glial cells (36–38). In contrast, the present study revealed, with the molecular changes in the diabetic retina, a significant decrease in synaptophysin (Fig. 3), the synaptic vesicle protein capable of maintaining the function of retinal neurons. Furthermore, AT1R signaling was shown to play a crucial role in the reduction of synaptophysin protein (Fig. 3). Pharmacologic studies using tetrodotoxin and glycine suggested the cellular origins of OPs as neurons with synapse formation in the inner retina including bipolar and amacrine cells (3,22,23), both of which develop a retinal neuronal network contributing to visual function. Synatophysin, a well-known marker for the presynapse, was shown to decrease with the progression of Parkinson's disease and Alzheimer's disease (19). In the retina as well, pathogenic conditions such as retinal detachment and inflammation caused reduction of synaptophysin (14,39). Mice deficient in synaptophysin exhibited a significant decrease in the number of synaptic vesicles (24). The neuron maintains its viability and activity by interacting with other neurons via synapses; however, synaptophysin knockouts were for the most part functionally compensated possibly because of biological redundancy (24). Although it is reasonable to think about the possibility of cooperative involvement of several other synaptic proteins, the diabetes-induced reduction of synaptopysin (Fig. 3) was attributable, at least in part, to the functional disturbance of neuronal activity in the diabetic retina. The currently observed suppression of synaptophysin decrease by AT1R blockade (Fig. 3) is likely to rescue the activity of the AT1R-bearing inner retinal neurons, leading to the improvement of OP changes (Fig. 2).

The present in vitro data (Figs. 4 and 5) further elucidated the detailed molecular mechanisms underlying the AT1R-mediated posttranscriptional decrease in synaptophysin observed in vivo (Fig. 3). Angiotensin II directly exerted its bioactivity to the neuronal cells via AT1R, leading to a posttranscriptional decrease in synatophysin (Fig. 4*A–F*), which mimicked the in vivo data (Fig. 3). Interestingly, angiotensin II/AT1R signaling proved to cause the activation of the UPS, leading to synaptophysin degradation in neuronal cells (Fig. 4*G–I*). Although the UPS was recently shown to play a role in the degradation of several synaptic proteins (25–27), the present data are the first to reveal the RAS-mediated UPS activation for synaptic protein degradation in neurons. Out of several signaling molecules in the downstream of AT1R, the phosphorylation of ERK, but not Akt or STAT3, was required for synaptophysin degradation (Fig. 5), suggesting that the UPS-dependent synaptophysin degradation is mediated by ERK activation. This is supported by several recent studies showing that the activation of the ERK pathway promoted the UPS-mediated degradation of the cell cycle protein Cdc25 (40,41) and the cell survival factor Bim (42). In the *Drosophila* eye, ERK signaling was shown to be required for the physiologic activity of Sina (seven in absentia), a key molecule for normal photoreceptor development (43). Interestingly, the mammalian homologues of *Drosophila* Sina, Siahs (seven in absentia homologues), proved to be synaptophysin-binding proteins functioning as E3 ubiquitin ligases to regulate the UPS-mediated degradation of synaptophysin (26). Reasonably, baseline ERK phosphorylation in the normal retina (Fig. 1) is likely to play a physiologic role in the UPS-mediated degradation of synaptophysin for the maintenance of synaptic plasticity (25–27). In the diabetic retina, however, excessive ERK activation mediated by AT1R (Fig. 1) is thought to induce the pathologic decline of synaptophysin (Fig. 3), contributing to neuronal dysfunction demonstrated by ERG (Fig. 2).

In the current study, diabetes-induced retinal dysfunction and synaptophysin downregulation were successfully reversed by AT1R signaling blockade in vivo (Figs. 2 and 3). Although future studies are required to determine whether angiotensin II/AT1R signaling leads to diabetes-induced neuronal damage systemically or locally in specific target organs, AT1R blockade has proven to be neuroprotective at least in the diabetic eye. Collectively, our present data show the possibility of AT1R blockade as a novel therapeutic strategy for neuronal dysfunction in vision-threatening diabetic retinopathy.

ACKNOWLEDGMENTS

The authors thank Masao Yoshikawa, Eiichiro Nagasaka (Mayo Company, Inazawa, Japan), and Hirobumi Tada (Yokohama City University, Yokohama, Japan) for expert advice and Haruna Koizumi and Taiga Shioda (Keio University, Tokyo, Japan) for technical assistance. This study was supported by the Japanese Ministry of Education, Culture, Sports, Science and Technology (Grant-in-Aid for Scientific Research [number 19791289] to T.K. and the 21st Century COE Program at Keio University).

This work was presented in part at the 2007 annual meeting of ARVO (Association for Research in Vision and Ophthalmology) in Fort Lauderdale, FL.

REFERENCES

1. Shirao Y, Kawasaki K: Electrical responses from diabetic retina. *Prog Retin Eye Res* 17:59–76, 1998
2. Kizawa J, Machida S, Kobayashi T, Gotoh Y, Kurosaka D: Changes of oscillatory potentials and photopic negative response in patients with early diabetic retinopathy. *Jpn J Ophthalmol* 50:367–373, 2006
3. Wachtmeister L: Oscillatory potentials in the retina: what do they reveal. *Prog Retin Eye Res* 17:485–521, 1998
4. Nagai N, Izumi-Nagai K, Oike Y, Koto T, Satofuka S, Ozawa Y, Yamashiro K, Inoue M, Tsubota K, Umezawa K, Ishida S: Suppression of diabetes-induced retinal inflammation by blocking the angiotensin II type 1 receptor or its downstream nuclear factor-κB pathway. *Invest Ophthalmol Vis Sci* 48:4342–4350, 2007
5. Danser AH, van den Dorpel MA, Deinum J, Derkx FH, Franken AA, Peperkamp E, de Jong PT, Schalekamp MA: Renin, prorenin, and immunoreactive renin in vitreous fluid from eyes with and without diabetic retinopathy. *J Clin Endocrinol Metab* 68:160–167, 1989
6. Sramek SJ, Wallow IH, Tewksbury DA, Brandt CR, Poulsen GL: An ocular renin-angiotensin system: immunohistochemistry of angiotensinogen. *Invest Ophthalmol Vis Sci* 33:1627–1632, 1992
7. Danser AH, Derkx FH, Admiraal PJ, Deinum J, de Jong PT, Schalekamp MA: Angiotensin levels in the eye. *Invest Ophthalmol Vis Sci* 35:1008–1018, 1994

8. Funatsu H, Yamashita H, Ikeda T, Nakanishi Y, Kitano S, Hori S: Angiotensin II and vascular endothelial growth factor in the vitreous fluid of patients with diabetic macular edema and other retinal disorders. *Am J Ophthalmol* 133:537–543, 2002
9. Funatsu H, Yamashita H: Pathogenesis of diabetic retinopathy and the renin-angiotensin system. *Ophthalmic Physiol Opt* 23:495–501, 2003
10. Funatsu H, Yamashita H, Nakanishi Y, Hori S: Angiotensin II and vascular endothelial growth factor in the vitreous fluid of patients with proliferative diabetic retinopathy. *Br J Ophthalmol* 86:311–315, 2002
11. Gilbert RE, Kelly DJ, Cox AJ, Wilkinson-Berka JL, Rumble JR, Osicka T, Panagiotopoulos S, Lee V, Hendrich EC, Jerums G, Cooper ME: Angiotensin converting enzyme inhibition reduces retinal overexpression of vascular endothelial growth factor and hyperpermeability in experimental diabetes. *Diabetologia* 43:1360–1367, 2000
12. Horio N, Clermont AC, Abiko A, Abiko T, Shoelson BD, Bursell SE, Feener EP: Angiotensin AT(1) receptor antagonism normalizes retinal blood flow and acetylcholine-induced vasodilatation in normotensive diabetic rats. *Diabetologia* 47:113–123, 2004
13. Phipps JA, Wilkinson-Berka JL, Fletcher EL: Retinal dysfunction in diabetic ren-2 rats is ameliorated by treatment with valsartan but not atenolol. *Invest Ophthalmol Vis Sci* 48:927–934, 2007
14. Kurihara T, Ozawa Y, Shinoda K, Nagai N, Inoue M, Oike Y, Tsubota K, Ishida S, Okano H: Neuroprotective effects of angiotensin II type 1 receptor (AT1R) blocker, telmisartan, via modulating AT1R and AT2R signaling in retinal inflammation. *Invest Ophthalmol Vis Sci* 47:5545–5552, 2006
15. Li DP, Chen SR, Pan HL: Angiotensin II stimulates spinally projecting paraventricular neurons through presynaptic disinhibition. *J Neurosci* 23:5041–5049, 2003
16. Dendorfer A, Thornagel A, Raasch W, Grisk O, Tempel K, Dominiak P: Angiotensin II induces catecholamine release by direct ganglionic excitation. *Hypertension* 40:348–354, 2002
17. Gallinat S, Busche S, Yang H, Raizada MK, Sumners C: Gene expression profiling of rat brain neurons reveals angiotensin II-induced regulation of calmodulin and synapsin I: possible role in neuromodulation. *Endocrinology* 142:1009–1016, 2001
18. Sun C, Li H, Leng L, Raizada MK, Bucala R, Sumners C: Macrophage migration inhibitory factor: an intracellular inhibitor of angiotensin II-induced increases in neuronal activity. *J Neurosci* 24:9944–9952, 2004
19. Zhan SS, Beyreuther K, Schmitt HP: Quantitative assessment of the synaptophysin immuno-reactivity of the cortical neuropil in various neurodegenerative disorders with dementia. *Dementia* 4:66–74, 1993
20. Hancock HA, Kraft TW: Oscillatory potential analysis and ERGs of normal and diabetic rats. *Invest Ophthalmol Vis Sci* 45:1002–1008, 2004
21. Li Q, Zemel E, Miller B, Perlman I: Early retinal damage in experimental diabetes: electroretinographical and morphological observations. *Exp Eye Res* 74:615–625, 2002
22. Heynen H, Wachtmeister L, van Norren D: Origin of the oscillatory potentials in the primate retina. *Vision Res* 25:1365–1373, 1985
23. Yonemura D, Kawasaki K: New approaches to ophthalmic electrodiagnosis by retinal oscillatory potential, drug-induced responses from retinal pigment epithelium and cone potential. *Doc Ophthalmol* 48:163–222, 1979
24. Spiwoks-Becker I, Vollrath L, Seeliger MW, Jaissle G, Eshkind LG, Leube RE: Synaptic vesicle alterations in rod photoreceptors of synaptophysin-deficient mice. *Neuroscience* 107:127–142, 2001
25. Chin LS, Vavalle JP, Li L: Staring, a novel E3 ubiquitin-protein ligase that targets syntaxin 1 for degradation. *J Biol Chem* 277:35071–35079, 2002
26. Wheeler TC, Chin LS, Li Y, Roudabush FL, Li L: Regulation of synaptophysin degradation by mammalian homologues of seven in absentia. *J Biol Chem* 277:10273–10282, 2002
27. Bingol B, Schuman EM: Synaptic protein degradation by the ubiquitin proteasome system. *Curr Opin Neurobiol* 15:536–541, 2005
28. Wilkinson-Berka JL: Angiotensin and diabetic retinopathy. *Int J Biochem Cell Biol* 38:752–765, 2006
29. Berka JL, Stubbs AJ, Wang DZ, DiNicolantonio R, Alcorn D, Campbell DJ, Skinner SL: Renin-containing Muller cells of the retina display endocrine features. *Invest Ophthalmol Vis Sci* 36:1450–1458, 1995
30. Senanayake P, Drazba J, Shadrach K, Milsted A, Rungger-Brandle E, Nishiyama K, Miura S, Karnik S, Sears JE, Hollyfield JG: Angiotensin II and its receptor subtypes in the human retina. *Invest Ophthalmol Vis Sci* 48:3301–3311, 2007
31. Brown L, Wall D, Marchant C, Semla C: Tissue-specific changes in angiotensin II receptors in streptozotocin-diabetic rats. *J Endocrinol* 154:355–362, 1997
32. Choi KC, Kim NH, An MR, Kang DG, Kim SW, Lee J: Alterations of intrarenal renin-angiotensin and nitric oxide systems in streptozotocin-induced diabetic rats. *Kidney Int Suppl* 60:S23–S27, 1997
33. Anderson S, Jung FF, Ingelfinger JR: Renal renin-angiotensin system in diabetes: functional, immunohistochemical, and molecular biological correlations. *Am J Physiol* 265:F477–F486, 1993
34. Hsieh TJ, Zhang SL, Filep JG, Tang SS, Ingelfinger JR, Chan JS: High glucose stimulates angiotensinogen gene expression via reactive oxygen species generation in rat kidney proximal tubular cells. *Endocrinology* 143:2975–2985, 2002
35. Zhang SL, Filep JG, Hohman TC, Tang SS, Ingelfinger JR, Chan JS: Molecular mechanisms of glucose action on angiotensinogen gene expression in rat proximal tubular cells. *Kidney Int* 55:454–464, 1999
36. Barber AJ, Lieth E, Khin SA, Antonetti DA, Buchanan AG, Gardner TW: Neural apoptosis in the retina during experimental and human diabetes: early onset and effect of insulin. *J Clin Invest* 102:783–791, 1998
37. Seki M, Tanaka T, Nawa H, Usui T, Fukuchi T, Ikeda K, Abe H, Takei N: Involvement of brain-derived neurotrophic factor in early retinal neuropathy of streptozotocin-induced diabetes in rats: therapeutic potential of brain-derived neurotrophic factor for dopaminergic amacrine cells. *Diabetes* 53:2412–2419, 2004
38. Feit-Leichman RA, Kinouchi R, Takeda M, Fan Z, Mohr S, Kern TS, Chen DF: Vascular damage in a mouse model of diabetic retinopathy: relation to neuronal and glial changes. *Invest Ophthalmol Vis Sci* 46:4281–4287, 2005
39. Sakai T, Calderone JB, Lewis GP, Linberg KA, Fisher SK, Jacobs GH: Cone photoreceptor recovery after experimental detachment and reattachment: an immunocytochemical, morphological, and electrophysiological study. *Invest Ophthalmol Vis Sci* 44:416–425, 2003
40. Eymin B, Claverie P, Salon C, Brambilla C, Brambilla E, Gazzeri S: p14ARF triggers G2 arrest through ERK-mediated Cdc25C phosphorylation, ubiquitination and proteasomal degradation. *Cell Cycle* 5:759–765, 2006
41. Wong J, Zhang J, Si X, Gao G, Luo H: Inhibition of the extracellular signal-regulated kinase signaling pathway is correlated with proteasome inhibitor suppression of coxsackievirus replication. *Biochem Biophys Res Commun* 358:903–907, 2007
42. Ley R, Balmanno K, Hadfield K, Weston C, Cook SJ: Activation of the ERK1/2 signaling pathway promotes phosphorylation and proteasome-dependent degradation of the BH3-only protein, Bim. *J Biol Chem* 278:18811–18816, 2003
43. Carthew RW, Neufeld TP, Rubin GM: Identification of genes that interact with the sina gene in Drosophila eye development. *Proc Natl Acad Sci U S A* 91:11689–11693, 1994

Clinical and Experimental Ophthalmology 2008; **36**: 386–396
doi: 10.1111/j.1442-9071.2008.01774.x

Letters to the Editor

Optical coherence tomographic findings of vitreomacular traction syndrome with macular hole retinal detachment

We report on two patients with the vitreomacular traction (VMT) syndrome whose vitreoretinal interface had a unique morphology. Case 1 was a 70-year-old woman who was referred to treat a macular hole retinal detachment (MHRD) in her right eye. Her visual acuity was 0.2, and ophthalmoscopy detected a MHRD of approximately three disc diameters (Fig. 1). Her refractive error (spherical equivalent) was +4.25 dioptres and the axial length was 21.02 mm. Optical coherence tomography (OCT) showed a perifoveal vitreous detachment with focal vitreal adhesions to the fovea, an incomplete posterior vitreous detachment (PVD), and two low reflective lines in the vitreous cavity (Fig. 1).

Vitrectomy was performed with phacoemulsification and implantation of an intraocular lens. After a complete PVD was created, the internal limiting membrane (ILM) in the area of the detached retina was peeled off (Fig. 1). The vitreous cavity was

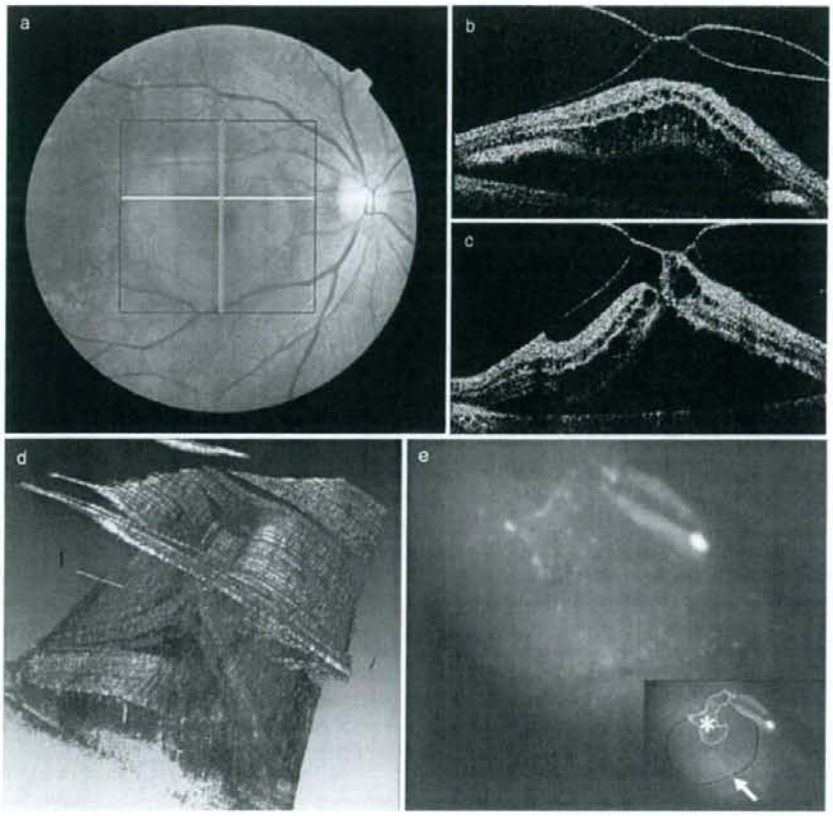

Figure 1 Fundus photograph and optical coherence tomographic (OCT) images showing macular hole retinal detachment in Case 1. (a) Fundus photograph showing a macular hole of approximately three disc diameters and a retinal detachment. The horizontal (yellow) and vertical (green) lines indicate the OCT scanned lines whose images are shown in (b) and (c), respectively. The square represents the scanned area shown in (d). (b) OCT image showing perifoveal vitreous detachment with the detached posterior vitreous cortex comprised of two low reflective lines (double-layered membrane) in the vitreous cavity. (c) OCT image showing perifoveal vitreous detachment with a macular hole and a focal vitreous adhesion to the fovea. (d) A three-dimensional OCT image showing the focal adhesion of the posterior vitreous surface causing it to form an inverted tent-like configuration over the macula and tent-like configuration of the macula. (e) Intraoperative photograph showing that the internal limiting membrane (ILM) was peeled off after removal of double-layered posterior vitreous membrane. Inset: The asterisk '*' indicates peeled ILM with triamcinilone crystals, and an arrow indicates the area where the ILM had been peeled off.

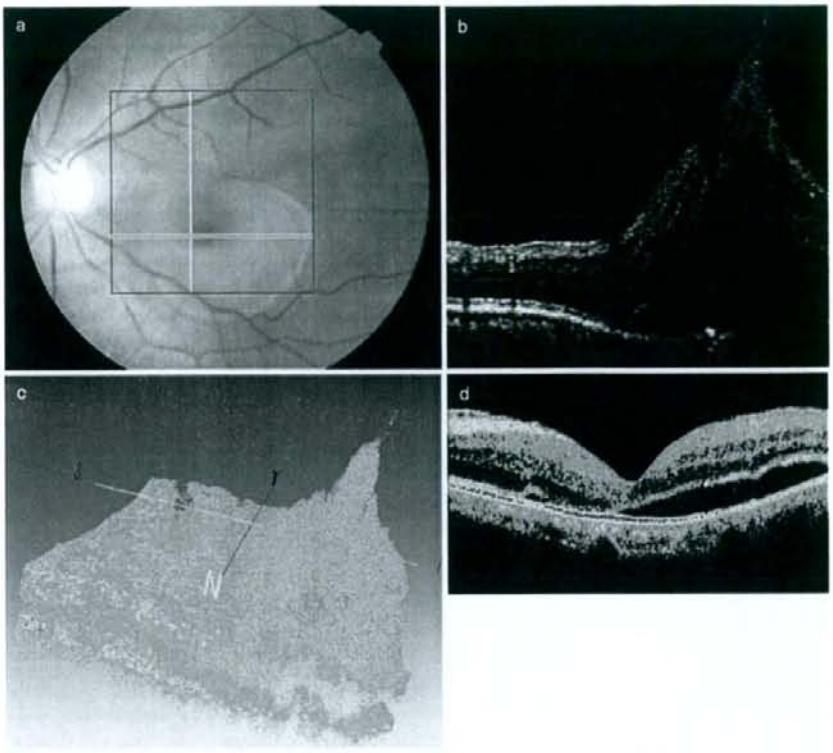

Figure 2. Fundus photograph and optical coherence tomographic (OCT) images showing macular hole retinal detachment (MHRD) in Case 2. (a) Fundus photograph showing a MHRD of approximately 2 × 3 disc diameters. The detached macular area is deviated inferiorly. The vertical (yellow) and horizontal (green) lines indicate the OCT scanned lines which are shown in (b) and (d) (after surgery), respectively. The square represents the OCT scanned area shown in (c). (b) OCT image showing focal attachment of the posterior vitreous to the perifovea that appears to exert a strong anterior-posterior tractional force. (c) A three-dimensional OCT image showing a focal adhesion of the posterior vitreous surface to a region inferior to the fovea causing a strong anterior-posterior tractional force and asymmetrical retinal detachment with its top deviated inferiorly. N = nasal, T = temporal. (d) One month postoperative OCT shows improved macular configuration with residual subretinal fluid.

filled with room air to tamponade the retina. Postoperatively, the retina was reattached, and the MH was closed. The visual acuity improved to 0.9 12 months after the vitrectomy (Fig. 1).

Case 2 was an 84-year-old man who was referred to treat a MHRD in his left eye. His visual acuity was 0.1, and ophthalmoscopy showed an inferiorly-deviated MHRD of approximately 2 × 3 disc diameters (Fig. 2). The left eye was pseudophakic and the axial length measured before MHRD was 23.17 mm. OCT showed a focal attachment of the posterior vitreous to the perifovea that appeared to cause a strong anterior-posterior tractional force (Fig. 2). Vitrectomy was successfully performed with the same procedure as in Case 1. The retinal and foveal configuration improved although some subretinal fluid remained. The visual acuity improved to 0.7 1 month after surgery (Fig. 2).

The VMT syndrome is characterized by an incomplete PVD with focal vitreomacular adhesions that distort the appearance and depress the function of the macula.[1] A persistent traction can lead to progressive macular oedema, thickening of the retina, and/or a RD.[1,2] In addition, a MHRD can occasionally develop even in non-myopic eyes as in our cases.

Morphological assessments of the vitreoretinal interface by OCT have led to a better understanding of how the anatomical change such as posterior staphyloma and vitreous traction can lead to MHRD or tractional retinoschisis in highly myopic eyes. Even in non-myopic eyes that do not have such an anatomical pathology, VMT may cause a MHRD.[3] But the rarity of these cases has prevented a comprehensive investigations on the morphology of the vitreomacular interface.

Our three-dimensional OCT study clearly illustrated the extensive morphological changes at the vitreomacular interface which played a role in development of MHRD in these two non-myopic eyes. A double-layered membrane attached to the fovea was considered to cause an unusual anterior-posterior traction thereby leading to the MHRD in Case 1. Because histology was not available, the exact composition of the membrane cannot be made, but the fact that the ILM was peeled off after removal of the membrane suggests that it was not part of the ILM. It may represent an epiretinal membrane (ERM) that was still attached to the detached posterior hyaloid membrane (PHM). Because the ERM was also firmly attached to the retina, traction by the detached PHM on the

FRM may have resulted in the RD. Further histological investigations will help in determining whether this membrane contained contractile elements or whether it was a vitreous schisis.

In Case 2, the off-centred vitreous adhesion probably caused an unusual anterior-posterior tractional force to develop the inferiorly deviated MHRD. Three-dimensional OCT in combination with intraoperative findings may be valuable ways to monitor the progress of the VMT syndrome and to clarify the mechanism of the secondary macular changes.

Acknowledgements

Support of this study was provided by Research Grants on Sensory and Communicative Disorders from the Ministry of Health, Labor and Welfare, Japan. No author has a proprietary interest in any material or method mentioned.

Machiko Tanimura MD, Kei Shinoda MD PhD, Yasuhiro Takaki MD, Kenichi Kimoto MD PhD, Kisaburo Yamada MD PhD and Kazuo Nakatsuka MD PhD

Department of Brain and Neuroscience, Division of Sensory and Locomotive Science, Ophthalmology, Oita University Faculty of Medicine, Yufu-shi, Oita, Japan

Received 16 December 2007, accepted 24 April 2008.

References

1. Smiddy WE, Michels RG, Green WR. Morphology, pathology, and surgery of idiopathic vitreoretinal macular disorders. A review. *Retina* 1990; **10**: 288–96.
2. Gass JMD. Vitreous traction maculopathy. In: Gass JMD, ed. *Stereoscopic Atlas of Macular Diseases*, 4th edn. St Louis: CV Mosby, 1997; 910–37.
3. Mavrofrides EC, Rogers AH, Truong S, Puliafito CA, Fujimoto JG. Vitreoretinal interface disorders. In: Schuman JS, Puliafito CA, Fujimoto JG, eds. *Optical Coherence Tomography of Ocular Diseases*, 2nd edn. Thorofare: SLACK Incorporated, 2004; 57–101.
4. Shimada N, Ohno-Matsui K, Baba T, Futagami S, Tokoro T, Mochizuki M. Natural course of macular retinoschisis in highly myopic eyes without macular hole or retinal detachment. *Am J Ophthalmol* 2006; **142**: 497–500.
5. Miyake Y. Macular hole retinal detachment and vitrectomy. *Ganka* 1994; **36**: 539–43 (in Japanese).

Optical coherence tomography in relentless placoid chorioretinitis

Relentless placoid chorioretinitis (RPC) was recently described[1] as a unique entity with atypical clinical findings and clinical course to both serpiginous choroidopathy and acute posterior multifocal placoid pigmented epitheliopathy (APMPPE). We report here on the changes in optical coherence tomographic (OCT) features in a patient suffering from RPC.

A 17-year-old healthy boy presented to the Ophthalmology Department at Hadassah University Hospital with an abrupt loss of left eye vision of one-day duration.

On examination visual acuity was 6/6 right eye and finger counting 2 m left eye. He had normal intraocular pressure and normal anterior segment examination. On funduscopy, faint subretinal lesions were noted in the macula and in the mid-peripheral retina of the right eye (Fig. 1a). In the left eye, an elevated yellowish macular lesion was noted (Fig. 1b). No lesions were seen elsewhere. Fluorescein angiography of the right eye showed areas of late hyperfluorescence in the macular area and in the mid-peripheral retina (Fig. 2a), while in the left eye, blocked fluorescence was noted in the macular area in the early phase with late hyperfluorescence (Fig. 2b). OCT was normal in the right eye, but in the left eye subretinal fluid with small area of pigment epithelial detachment was detected in the macular area (Fig. 3a). Also, hyper-reflectivity of the nuclear retinal layers was noted, namely, the ganglion cell layer, the inner and the outer nuclear layers. Full-field ERG, EOG and colour vision were normal. Systemic medical work-up for infectious and inflammatory aetiology, including complete blood count, erythrocyte sedimentation rate, C-reactive protein, kidney function tests, liver function tests and serology for herpes viruses, syphilis, HIV and Lyme disease, was normal. Antinuclear antibodies were not detected, and angiotensin-converting enzyme level and chest X-ray were normal.

Ten days later, the patient presented with spontaneous improvement in left eye vision to 6/10. On examination, anterior segments were normal, +1 vitreous cells were noted with bilateral placoid pigmented chorioretinal scars and active fluffy diffuse subretinal lesions in the mid and far periphery. There was resolution of the left macular yellow lesion with fine pigmentary changes instead. The lesions looked similar to those seen with APMPPE and there was posterior pole involvement. Prednisolone (1 mg/kg/day) was started with a tapering regimen. During the ensuing months and despite the steroid therapy, active lesions were continuously appearing with

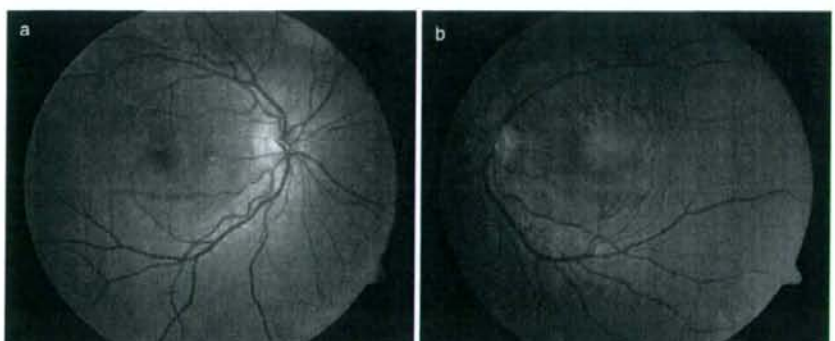

Figure 1 (a) Colour fundus photography of the right eye, showing faint subretinal lesions in the macular area temporal to the fovea and in the mid-peripheral retina. (b) Colour fundus photography of the left eye showing an elevated yellowish macular lesion.

Acta Ophthalmologica

Diagnosis / Therapy in Ophthalmology

Frosted branch angiitis associated with streptococcal infection: optical coherence tomography as a follow-up tool

Hirofumi Kono,[1] Junko Ikewaki,[1] Kenichi Kimoto,[1] Masatoshi Furushima,[1] Yasuo Yae,[2] Kei Shinoda[1] and Kazuo Nakatsuka[1]

[1]Department of Brain and Neuroscience, Division of Sensory and Locomotive Science, Ophthalmology, Faculty of Medicine, Oita University, Oita, Japan
[2]Yae Eye Clinic, Oita, Japan

Acta Ophthalmol.

doi: 10.1111/j.1755-3768.2008.01335.x

A 7-year-old boy presented with decreased vision and conjunctivitis in both eyes. He had a flu-like episode with fever about 2 weeks earlier, and the skin of both palms had peeled off. His visual acuity (VA) was 0.15 OD and 0.1 OS. Slit-lamp examination showed conjunctival and ciliary injection, cells in the anterior chamber, flare and fine keratic precipitates bilaterally. Ophthalmoscopy revealed diffuse, white perivascular sheathing of the arteries and veins, tortuous and dilatated veins, scattered retinal haemorrhages and papilloedema in both eyes (Fig. 1A). Fluorescein angiography demonstrated extensive dye leakage from almost all vessels (Fig. 1B) and both optic discs were hyperfluorescent in the late phase. Indocyanine green angiography (ICGA) showed a mottled background pattern, staining of the vessels especially in the posterior pole, and hypofluorescence of the discs with blurred margins (Fig. 1C). Optical coherence tomography (OCT Model 2000; Carl Zeiss Meditec, Inc., Dublin, CA, USA) showed a clear serous detachment and oedema in the macula (Fig. 1D, E). Goldmann perimetry showed an enlarged blind spot. The amplitudes of the a- and b-waves and the oscillatory potentials of the electroretinograms (ERGs) elicited by a bright flash were significantly reduced (Fig. 1F).

Systemic examinations disclosed no abnormal findings except for high titres of anti-streptolysin O (ASO, 1830×) and anti-streptokinase (ASK, 5120×).

From these findings, the subject was diagnosed with frosted branch angiitis (FBA). He was treated with topical 0.1% betamethasone and 1.0% atropine along with i.v. prednisolone (580 mg/day) for 3 days and subsequently oral prednisolone for 15 days (total 165 mg). Three days later, the aqueous inflammation and the perivascular sheathing were markedly reduced. Thereafter, OCT and ophthalmoscopy of the macular area showed a resolution of the oedema followed by the appearance of a star-shaped figure (Fig. 1G, H). The subject's ERGs were markedly improved but were still not normal (Fig. 1I). The serous detachment (Fig. 1J, K) and finally exudates disappeared.

Despite the rapid improvement in the appearance of the retina, the patient's VA improved much more slowly and attained 1.0 only after 3 months. Fundus angiography at that time demonstrated the complete resolution of all abnormal findings.

The increase in the number of cases diagnosed as FBA raises questions about whether this disorder represents a distinct clinical syndrome or merely a clinical sign of eyes with inflammatory conditions. From their descriptions in the literature, cases diagnosed as FBA are characterized by bilateral, perivascular retinal blood vessel sheathing, retinal haemorrhages and oedema of different degrees, panuveitis and papilloedema (Walker et al. 2004). Our case had diffuse angiitis involving the vessels of the macular and peripheral retina and the choroid. Anterior uveitis and papilloedema were also present. The abnormal ICGA findings suggested that the choroid was also altered, which probably accounts for the decreased a-waves on ERG. The reduced b-waves indicated alterations to the inner retina. Whether these findings are also found in other chorioretinal inflammatory diseases is yet to be determined. The prevalence of FBA is reported to be higher in Asians than in White populations (Walker et al. 2004).

Despite the marked panophthalmic inflammation, the eye responded well to steroids. Our subject's VA recovered to normal levels, but some FBA subjects suffer a permanent loss of vision caused by macular scarring (Kleiner et al. 1988; Walker et al. 2004).